KU LEUVEN

HERCORE: Highly Efficient and quasi-Realistic CORonal and coronal mass Ejection modeling

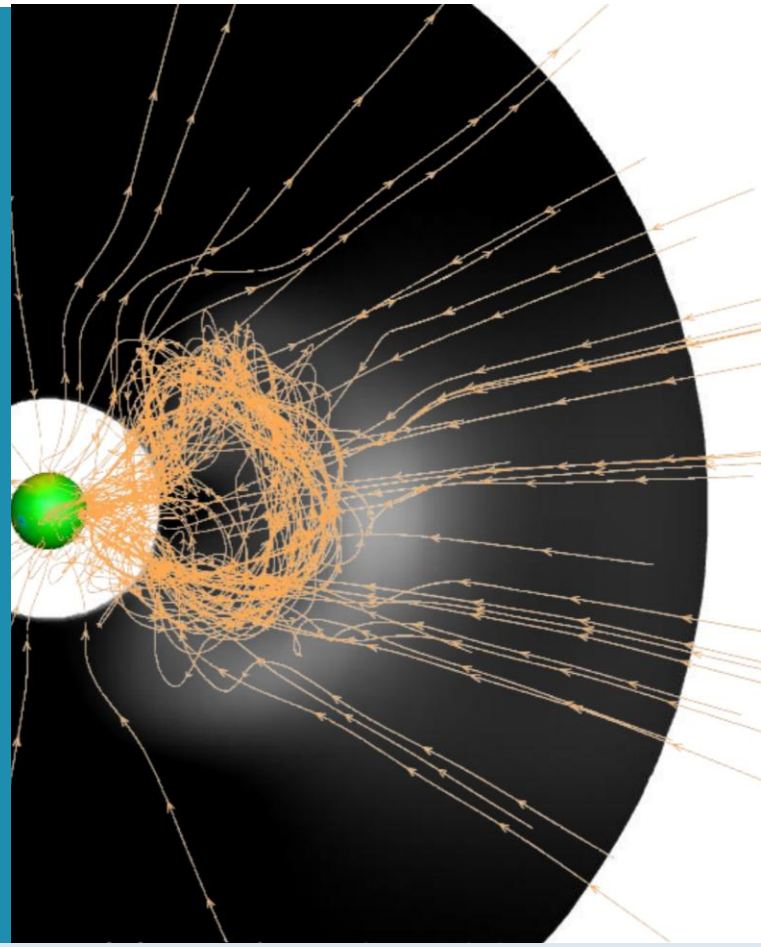

Dr. Haopeng Wang

Postdoctoral Researcher, KU Leuven (Supervisor: Stefaan Poedts)

Ph.D., National Space Science Center, UCAS (Supervisor: Xueshang Feng)

E-mail: haopeng.wang1@kuleuven.be

KU Leuven, 29/09/2025

Outline

- Challenges in MHD coronal modeling
- Fully implicit, quasi-steady state MHD coronal models **COCONUT** and predecessor of **SIP-IFVM**
- Fully implicit, time-evolving MHD coronal models **COCONUT** and **SIP-IFVM**
- Faster-than-real-time MHD modeling of CME propagation through the sub-Alfvénic corona

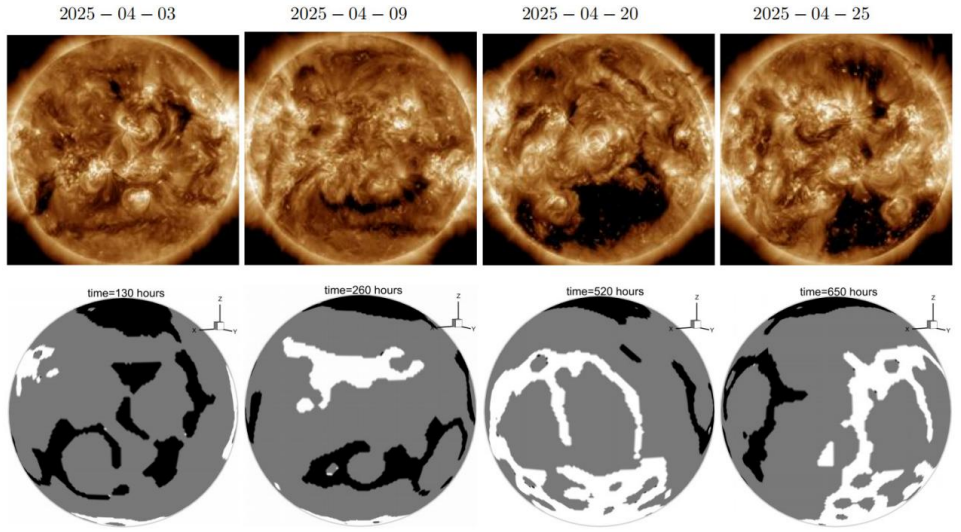

SDO/AIA observation and simulated open-field region from **COCONUT**

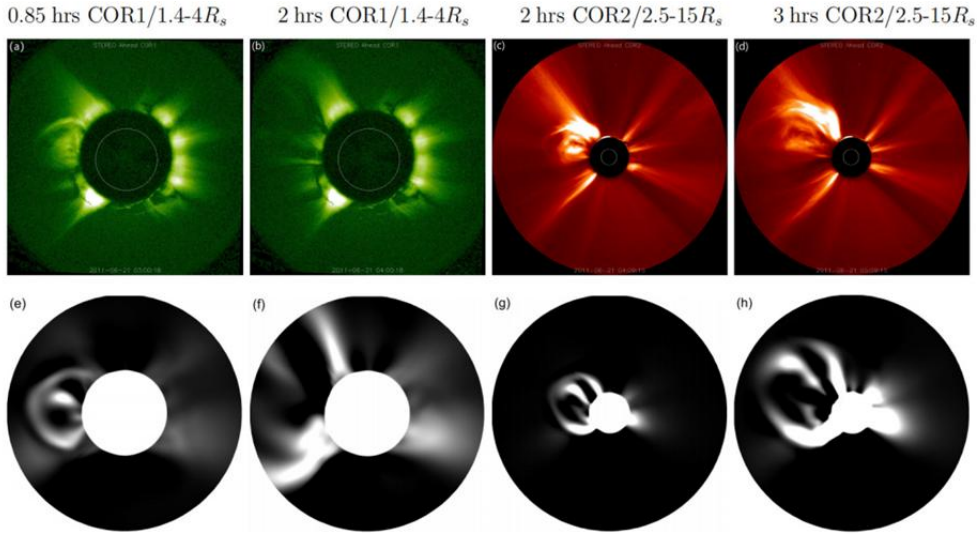

STEREO-A observation and CME simulation by **SIP-IFVM**

Our goal: Solar-terrestrial space and space weather forecasting

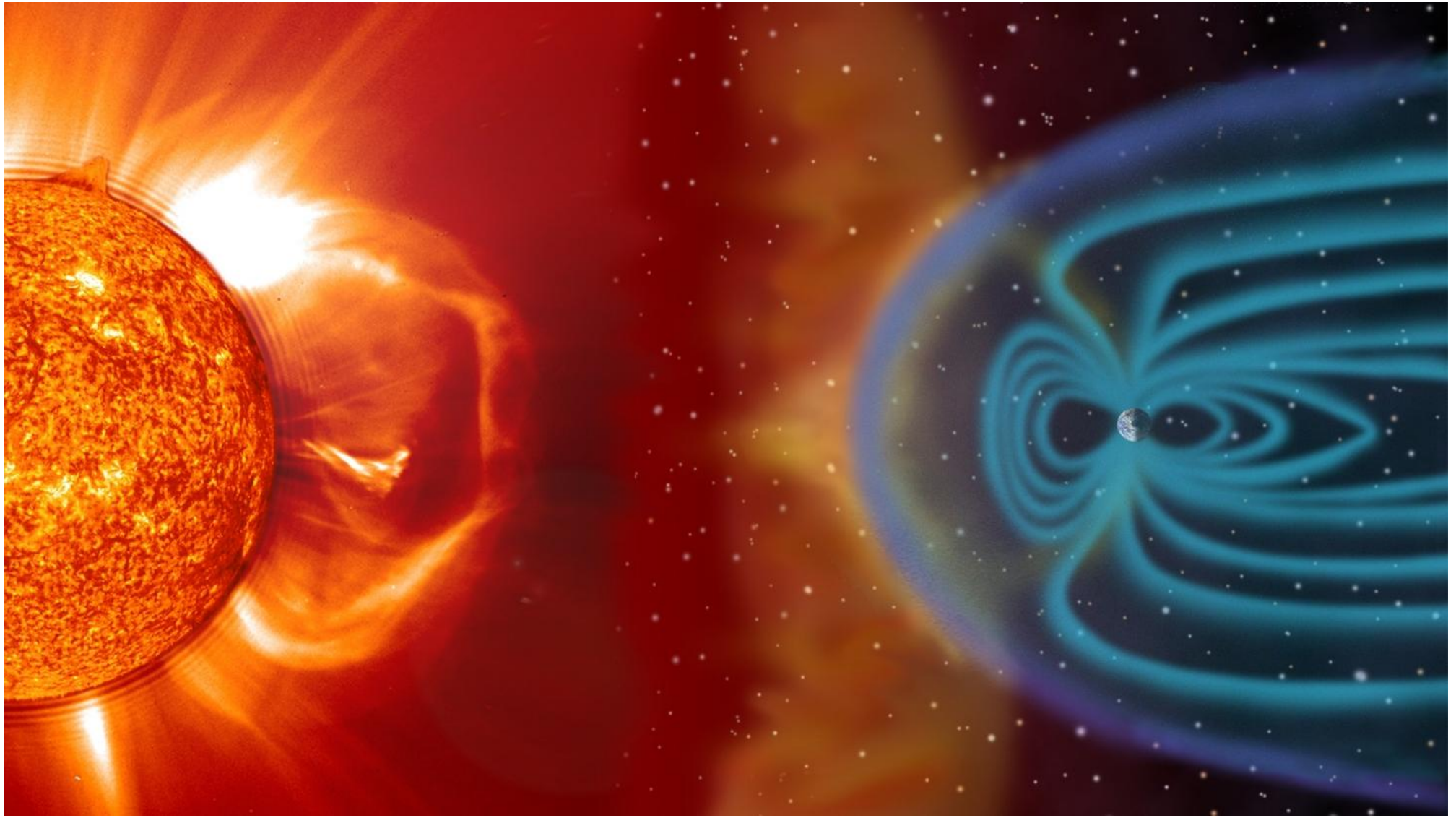

Our society suffers from severe space weather:

1989 Quebec blackout

Satellite electronics damage during the 2003 “Halloween Storm”

A geomagnetic storm in February 2022 caused loss of up to 40 out of 49 Starlink satellites.

et al.

Critical and extremely challenging work: Efficient time-evolving coronal modeling

Color-enhanced image (the saturation was increased by 50×) of the white-light observation of total solar eclipse of 2008 August 1 (Pasachoff et al. 2009)

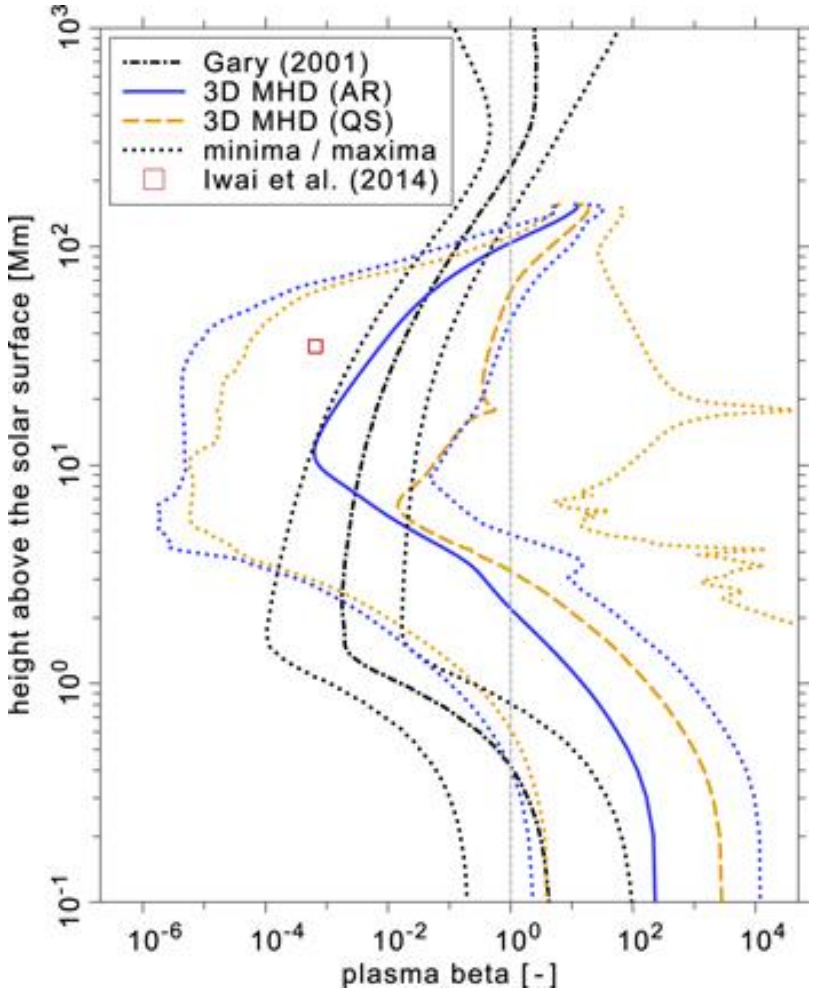

Illustration of the plasma β near the solar surface (Bourdin 2017).

Challenges and advantages of coronal and solar wind MHD modeling

Challenges

- Uncertain boundary data: incomplete and noisy solar magnetograms.
- Coronal heating problem: poorly understood mechanisms.
- Multi-scale physics: difficult to resolve both fine coronal structure and global solar wind.
- Numerical stability & efficiency: stiff low-β regions require costly schemes.
- Limited microphysics: small-scale or kinetic effects are not fully captured.
- CME initiation & propagation: hard to capture realistic reconnection and magnetic topology.
- Lower-atmosphere coupling: simplified treatment of chromosphere/transition region.

Advantages:

- Physics-based: self-consistent plasma dynamics (mass, momentum, energy, magnetic flux).
- Global coverage: Sun-to-Earth, capturing corona and heliosphere structures.
- Predictive: forecasts solar wind, CMEs, and space weather events.
- Flexible & diagnostic: integrates multiple processes and supports observational comparisons.
- Coupled processes: includes magnetic fields, waves, and thermodynamics simultaneously.
- Operational utility: supports space weather forecasting.
- Insightful: helps test hypotheses about coronal heating, solar wind acceleration, and heliospheric structures.

Challenges in MHD coronal modeling: low-β issues

- Nonphysical **negative thermal pressure** is prone to occur in the floating-point calculation process of deriving thermal pressure from energy density.
- Extremely **small time-step length** determined by the Courant-Friedrichs-Lewy (CFL) restriction.
- **Non-zero magnetic field divergence error** leads to anomalous Lorentz force parallel to the magnetic field, leading to severe stability problems.
- A solver suitable for **both the incompressible low- and compressible high-speed flows** is required.

$$\beta = \frac{p}{0.5 * \mathbf{B}^2}$$

Challenges in MHD coronal modeling: low-β issues

- Nonphysical **negative thermal pressure** is prone to occur in the floating-point calculation process of deriving thermal pressure from energy density.

- Positivity-preserving reconstruction method
- **Decomposed MHD equations**
- **Decomposed energy equation**
- Appropriate numerical flux solver

$$p = (\gamma - 1)\left(E - \frac{1}{2}(\rho \boldsymbol{V}^2 + \boldsymbol{B}^2)\right)$$

$$\beta = \frac{2p}{\boldsymbol{B}^2}$$

catastrophic cancellation

$$(\boldsymbol{B} + \varepsilon\boldsymbol{B})^2 - \boldsymbol{B}^2 \equiv \varepsilon\boldsymbol{B}^2$$

$\varepsilon\boldsymbol{B}$ means the discretization error of $\boldsymbol{B}$.
During the 2nd or 3rd order spatial discretization procedure, $\varepsilon\boldsymbol{B}^2 \equiv p$ for low β cases.

Challenges in MHD coronal modeling: low-β issues

- Extremely **small time-step length** determined by the Courant-Friedrichs-Lewy (CFL) restriction.

- Implicit temporal integration method enable large time steps exceed CFL stability restriction

$$\triangle \mathrm{t} = \mathrm{CFL} \cdot \frac{dh}{c_f}$$

dh: characteristic cell size

c_f: Maximum wave velocity in current cell

Usually, CFL < 1 for explicit scheme.
The time step length $\triangle$t decreases with magnetic field strength increasing. $\triangle$t may be less than 10^{-4} hours for low-β MHD simulations.

Challenges in MHD coronal modeling: low-β issues

- **Non-zero magnetic field divergence error** leads to anomalous Lorentz force parallel to the magnetic field, leading to severe stability problems.

- Divergence-free magnetic field reconstruction methods
- Appropriate discretization of Powell source terms
- Hyperbolic generalized Lagrange multiplier method

$$\frac{\partial \psi}{\partial t} + c_h^2 \nabla \cdot \mathbf{B} = 0$$

$$\frac{\partial \mathbf{B}}{\partial t} + \nabla \times \mathbf{E} + \nabla \psi = 0$$

$$\mathbf{F} = \mathbf{J} \times \mathbf{B} = \nabla \times \mathbf{B} \times \mathbf{B}$$
$$= -\nabla\left(\frac{B^2}{2}\right) + (\mathbf{B} \cdot \nabla)\mathbf{B} + \mathbf{B}(\nabla \cdot \mathbf{B})$$

Implicit **quasi-steady coronal** model: predecessor of **SIP-IFVM**

Notable improvement in efficiency and stability of two implicit coronal MHD models: 1.016×10^6 cells, 192 CPUs

Carrington rotation	β_{min}	CFL	$\triangle$ t(h)	τ_{wall}^{Exp}(h)	τ_{wall}^{Imp}(h)	Speed up ratio(x)
①CR 2172	1.6×10^{-5}	$0.5 - 475.5$	$6.0 \times 10^{-5} - 5.7 \times 10^{-2}$	74.08	0.33	224.5
①CR 2210	9.4×10^{-4}	$0.5 - 155.5$	$4.5 \times 10^{-4} - 0.14$	7.53	0.18	41.9
①Manuf-actured test	4.6×10^{-7}	$0.5 - 2800.5$	$1.0 \times 10^{-5} - 5.6 \times 10^{-2}$		0.61	>1000
②CR 2177	7.0×10^{-5}	$0.5 - 355.5$	$8.6 \times 10^{-5} - 6.2 \times 10^{-2}$		0.79	
②CR 2212	1.0×10^{-3}	$0.5 - 105.5$	$7.7 \times 10^{-4} - 0.16$		0.52	

Xueshang Feng, Haopeng Wang, Changqing Xiang et al.: 2021, Magnetohydrodynamic modeling of the solar corona with an effective implicit strategy. ApJS 257(2):1-23.

Haopeng Wang, Changqing Xiang, Xiaojing Liu et al.: 2022b, Implicit solar coronal magnetohydrodynamic (MHD) modeling with a low-dissipation hybridized AUSM-HLL Riemann solver. ApJ 935(1):1-20.

Haopeng Wang, Jingmin Zhao, Jiakun Lv et al.: 2022, A solenoidality-preserving variational reconstruction method and its application to solar coronal MHD modeling (in Chinese) . Chin . J. Geophys 65(8):1-17.

Implicit **quasi-steady coronal** model: predecessor of **SIP-IFVM**

Comparation between results calculated by the E-MHD and improved I-MHD models

CR 2172

$\phi = 143° - 323°$

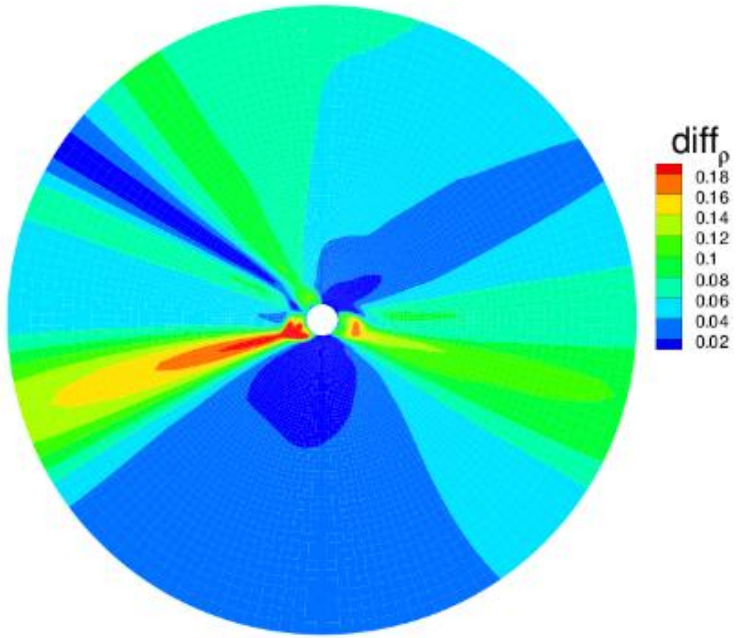

CR 2210

$\phi = 111° - 291°$

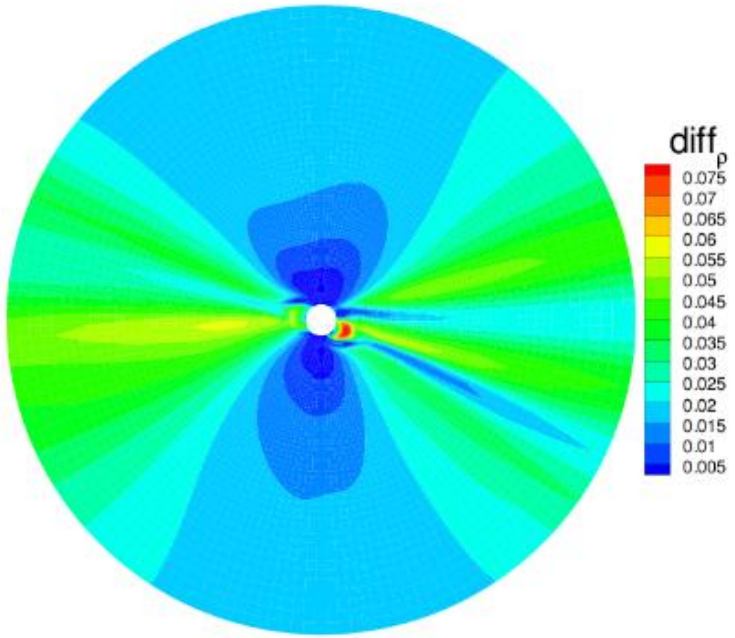

$$\mathrm{diff}_{\rho,i} = \left|\rho_i^{\mathrm{Imp}} - \rho_i^{\mathrm{Exp}}\right| / \rho_i^{\mathrm{Imp}}$$

$$\mathrm{diff}_{\mathrm{ave},\rho} = \frac{\sum_{i=1}^{N}\left|\rho_i^{\mathrm{Imp}} - \rho_i^{\mathrm{Exp}}\right|}{\sum_{i=1}^{N}\rho_i^{\mathrm{Imp}}} \approx 5.23\%, 1.97\%$$

The relative differences of steady-state proton number density on the meridional planes of of $\phi = 143° - 323°$ for CR 2172 (left) and $\phi = 111° - 291°$ for CR 2210 (right). They are calculated from the steady-state results of the E-MHD and improved I-MHD models.

Implicit **quasi-steady coronal** model: predecessor of **SIP-IFVM**

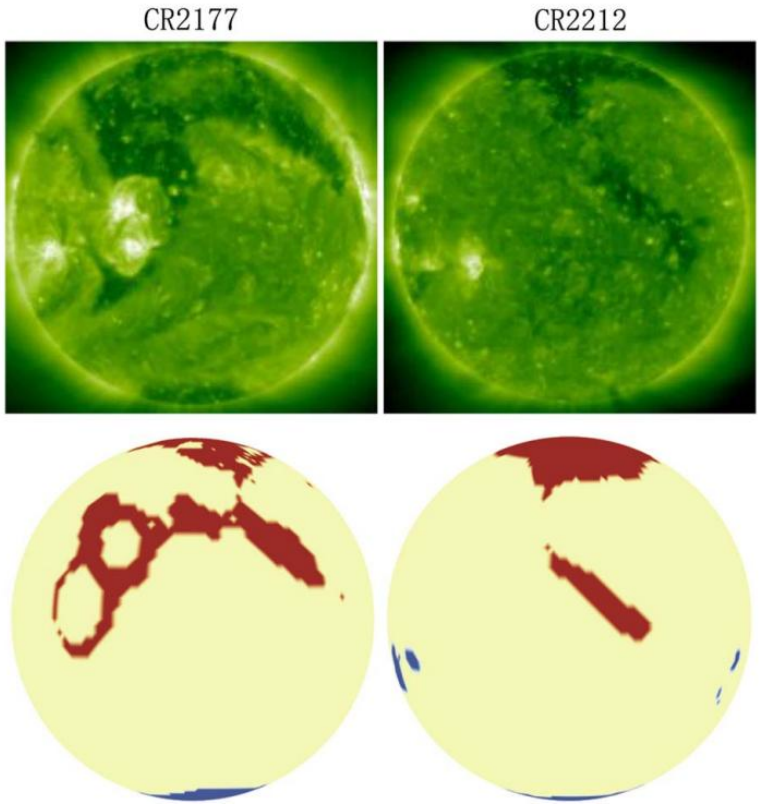

Full-disk images from EUVI/STEREO-A with the channel of 195 Å on 2016 May 4 (top left) and 2018 December 19 (top right), and full-disk images of the modeled open-field for CRs 2177 (bottom left) and 2212 (bottom right). The open-field regions with magnetic field pointing away from the Sun are painted red, and these regions with magnetic field pointing toward the Sun are painted blue.

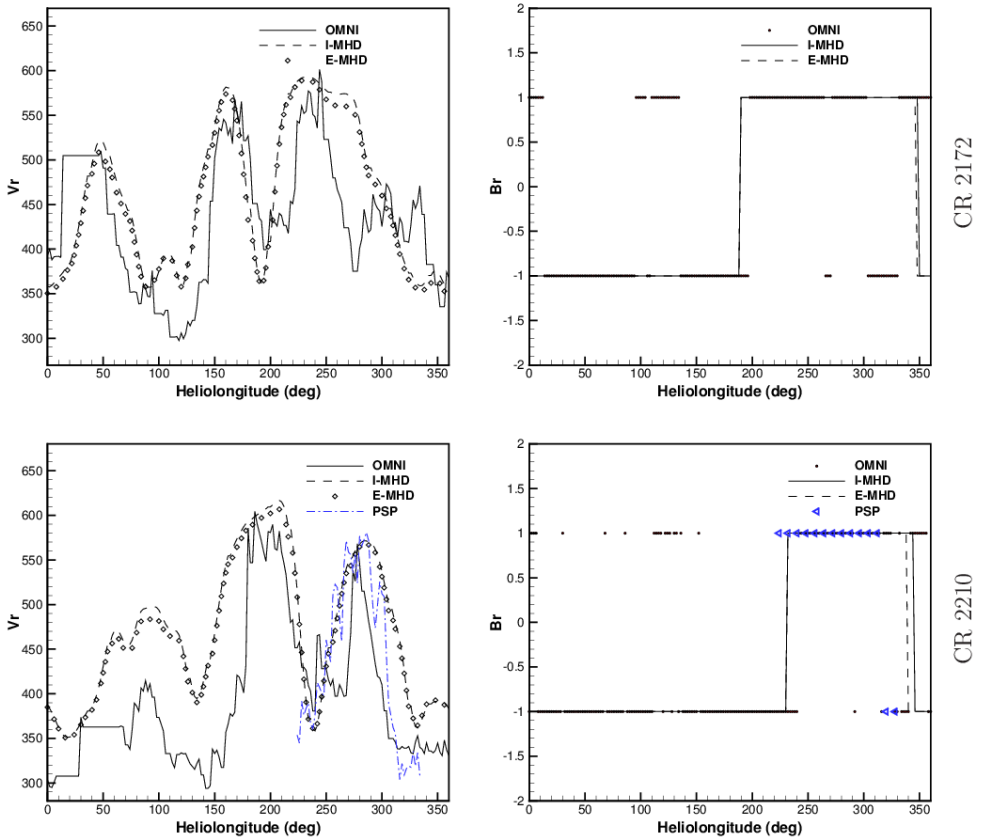

Temporal profiles of the modeled and observed radial speed Vr (km/s) (left) and the radial magnetic field polarities (right) with "-1" denoting the field pointing to the Sun and "+1" the field directing away from the Sun at 20 R_s for CRs 2172 (top) and 2210 (bottom).

Implicit **quasi-steady coronal** model: **COCONUT**

- **Unstructured geodesic grid mesh [Brchnelova et al. 2022]**

Brchnelova, M., Zhang, F., Leitner, P., et al. 2022b, J. Plasma Phys., 88, doi:10.1017/S0022377822000241

- Flexible in mesh division
- Avoid degeneracy at the poles

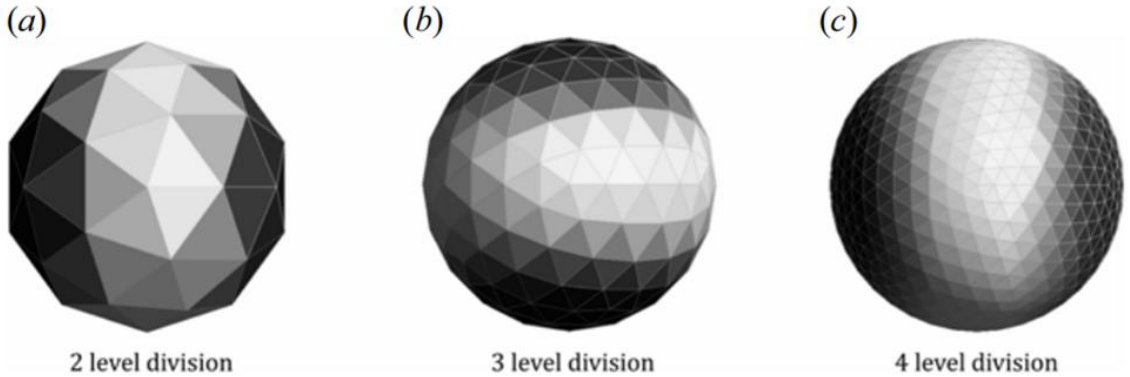

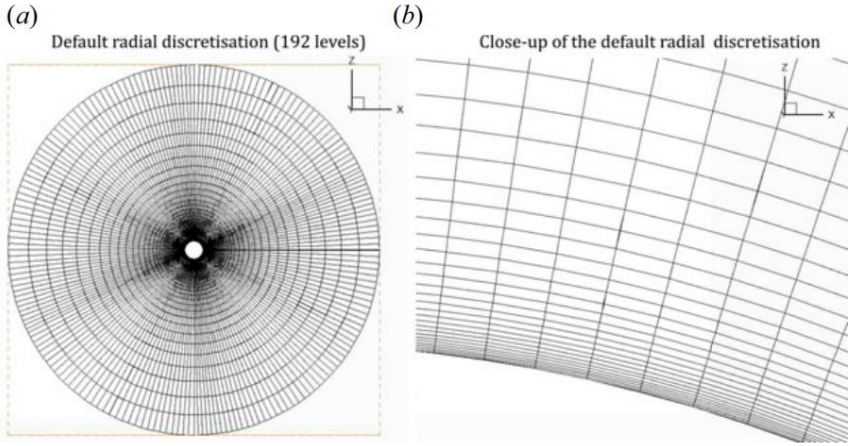

Implicit **quasi-steady coronal** model: **COCONUT**

- **Impact of the input magnetic map on simulation results [Perri et al. 2023]**

Barbara Perri et al 2023 ApJ 943 124, doi:10.3847/1538-4357/ac9799

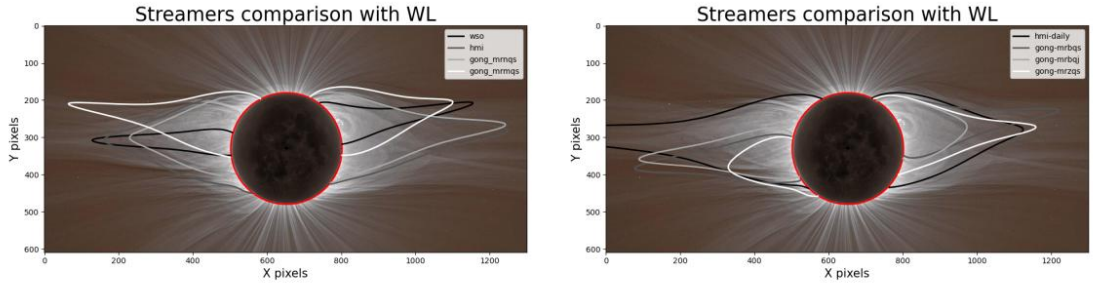

(a) Carrington frame diachronic maps.

(b) Synchronic frame maps.

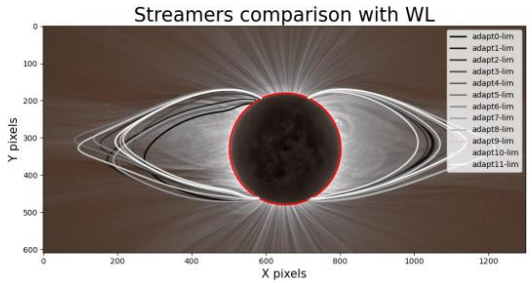

(c) GONG-ADAPT realisations.

Implicit **quasi-steady coronal** model: **COCONUT**

- **Validation method of Wagner et al. (2022) used in the case of the 2019 total solar eclipse [Kuźma et al. 2023]**

Błażej Kuźma et al 2023 ApJ 942 31, doi:10.3847/1538-4357/aca483

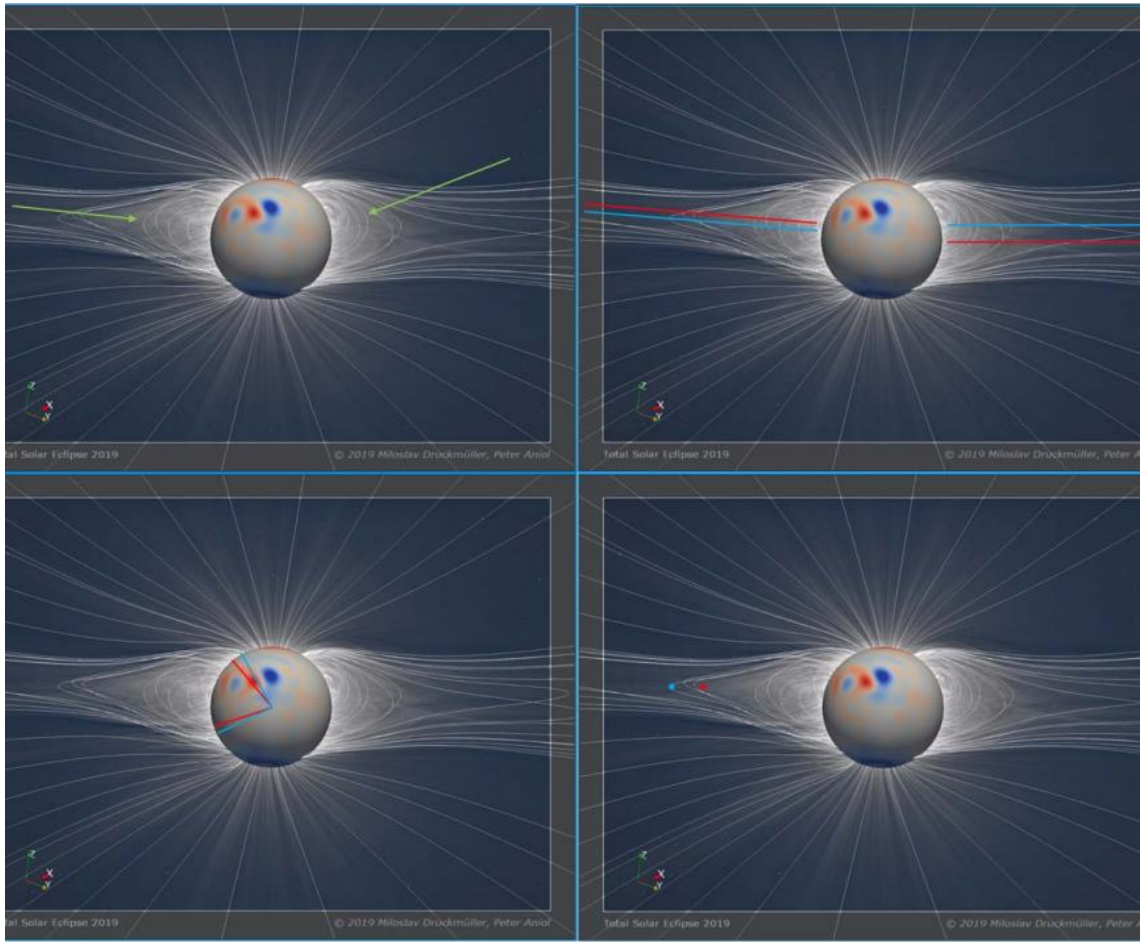

Implicit **quasi-steady coronal** model: **COCONUT**

- **Two-fluid ion-neutral global coronal modelling [Brchnelova et al. 2023]**

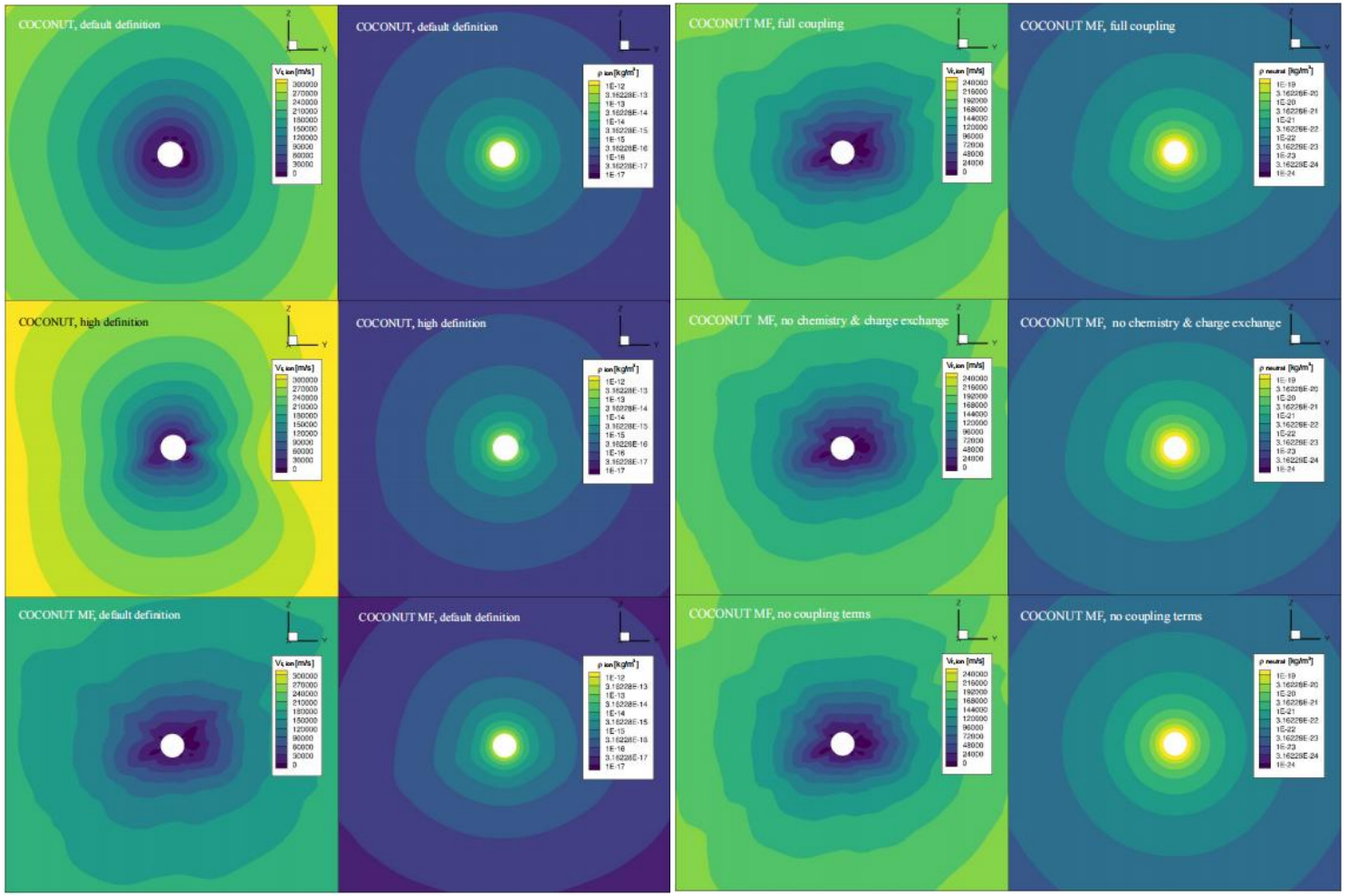

Brchnelova, Michaela et al 2023 A&A 678 A117, doi: 10.1051/0004-6361/202346525

Fully implicit, time-evolving MHD coronal models COCONUT and SIP-IFVM

COCONUT:

- Unstructured geodesic grid mesh
- Implicit: GMRES solver
- Decomposed energy strategy enhances stability for addressing **time-evolving low-β issues.**
- Multi-fluid module enables higher fidelity of the simulation results.

SIP-IFVM:

- Six-component structured grid system
- Implicit: Improved parallel LU-SGS solver
- Extended magnetic field decomposition strategy effectively tackles **time-evolving low-β issues.**
- Improved ESDIRK2 algorithm balances high temporal accuracy and numerical stability.

Fully implicit, time-evolving MHD coronal models COCONUT and SIP-IFVM

COCONUT:

- **Unstructured geodesic grid mesh**
  - Flexible in mesh division
  - Avoid degeneracy at the poles

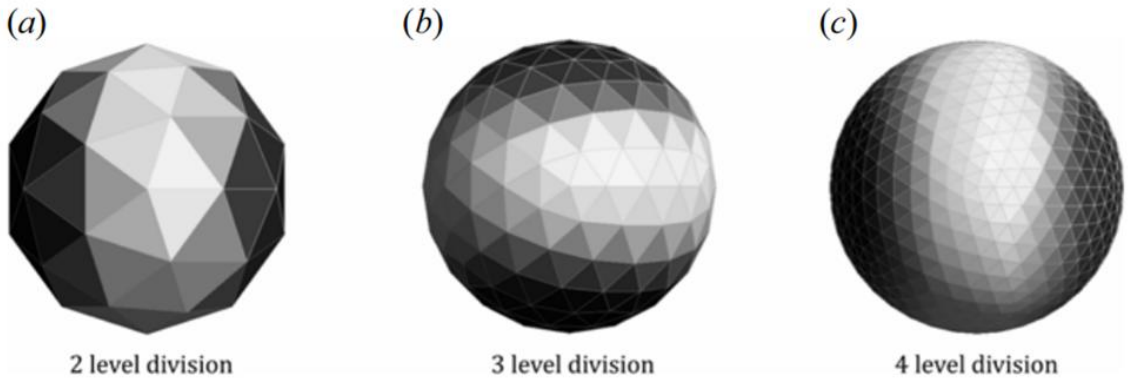

SIP-IFVM:

- Six-component structured grid system
  - All components calculated in low-latitude domain
  - Free of polar singularity

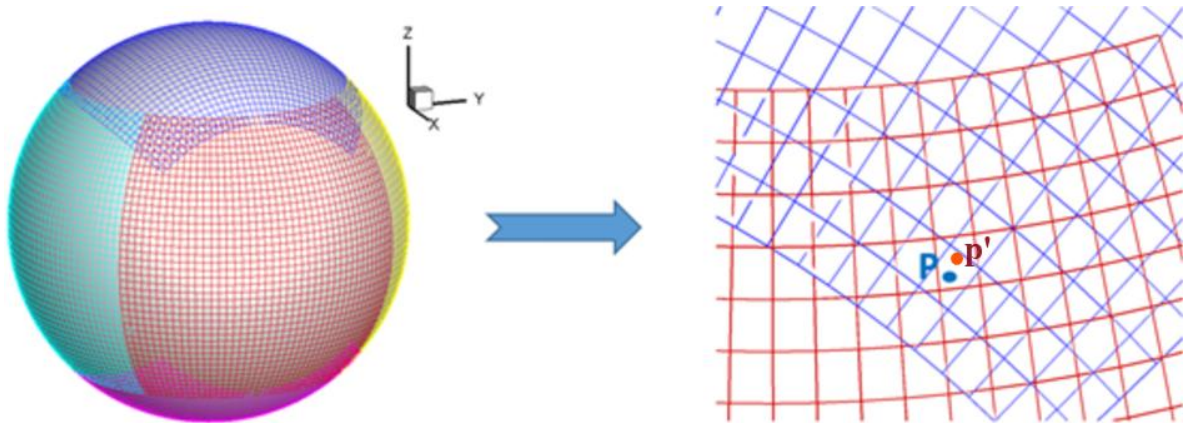

Fully implicit, time-evolving MHD coronal models COCONUT and SIP-IFVM

COCONUT:

- Implicit: Parallel GMRES solver
  - Global matrix solving technique
  - Converge with less iterations, require more memory
  - Simulate the coronal evolution during **a full CR within only 9 hours** (1080 CPU cores, ~1.5M cells, time step is 10 minutes.)

SIP-IFVM:

- Implicit: Improved parallel LU-SGS solver
  - Approximate factorization method, require less memory
  - Accurate synchronous data communication
  - Enhance the diagonal dominance of the Jacobian matrix
  - **More than 80 times faster** than real-time coronal evolution (192 CPU cores, ~1M cells, time step is between 3 and 4 minutes.)

$$V_i \frac{\triangle \mathbf{U}_i^n}{\triangle t} + \mathbf{R}_i^{n+1} = \mathbf{0}; \qquad \mathbf{A}\,\triangle \mathbf{U}^n = \mathbf{R}^n, \triangle \mathbf{U}^n = \mathbf{U}^{n+1} - \mathbf{U}^n$$

- $\mathbf{A}$ is the Jacobian matrix, a large sparse coefficient matrix
- $\mathbf{U}$ is the solution vector

Fully implicit, time-evolving MHD coronal models COCONUT and SIP-IFVM

COCONUT:

- Decomposed energy strategy

$$
\begin{cases}
\dfrac{\partial \rho}{\partial t} + \nabla \cdot (\rho \mathbf{v}) = 0, \\
\dfrac{\partial (\rho \mathbf{v})}{\partial t} + \nabla \cdot \left[\rho \mathbf{v}\mathbf{v} + \left(p + \dfrac{\mathbf{B}^2}{2} \right) \mathbf{I} - \mathbf{B}\mathbf{B} \right] = \mathbf{0}, \\
\dfrac{\partial E_1}{\partial t} + \nabla \cdot \left[(E_1 + p)\,\mathbf{v} \right] = -\mathbf{B} \cdot (\mathbf{v} \cdot \nabla \mathbf{B}) + \mathbf{v} \cdot (\mathbf{B} \cdot \nabla \mathbf{B}) \\
\dfrac{\partial \mathbf{B}}{\partial t} + \nabla \cdot (\mathbf{v}\mathbf{B} - \mathbf{B}\mathbf{v} + \psi \mathbf{I}) = \mathbf{0}, \\
\dfrac{\partial \psi}{\partial t} + V_{\mathrm{ref}}^2 \, \nabla \cdot \mathbf{B} = 0 .
\end{cases}
$$

$$
E_1 = \frac{p}{\gamma - 1} + \frac{\rho \mathbf{v}^2}{2}
$$

Haopeng Wang, Stefaan Poedts, Andrea Lani et al., 2025, COCONUT: A time-evolving coronal model with an energy decomposition strategy. 1-12. [arXiv:2508.20423]

SIP-IFVM:

- Extended magnetic field decomposition strategy

$$
\begin{cases}
\dfrac{\partial \rho}{\partial t} + \nabla \cdot (\rho \mathbf{v}) = 0 \\
\dfrac{\partial (\rho \mathbf{v})}{\partial t} + \nabla \cdot \left[\rho \mathbf{v}\mathbf{v} + \left(p + \dfrac{\mathbf{B}^2}{2} - \dfrac{\mathbf{B}_{00}^2}{2} \right) \mathbf{I} - \mathbf{B}\mathbf{B} + \mathbf{B}_{00}\mathbf{B}_{00} \right] = -\nabla \cdot (\mathbf{B}_1 + \mathbf{B}_{01})\,\mathbf{B} \\
\dfrac{\partial E_1}{\partial t} + \nabla \cdot \left[\left(E_1 + p_{T1} + \mathbf{B}_1 \cdot \mathbf{B}_0 \right) \mathbf{v} - \mathbf{B}\,(\mathbf{v} \cdot \mathbf{B}_1) \right] = -\nabla \cdot (\mathbf{B}_1 + \mathbf{B}_{01})\,(\mathbf{v} \cdot \mathbf{B}_1) \\
\quad - \mathbf{B}_1 \cdot \dfrac{\partial \mathbf{B}_0}{\partial t} - \mathbf{v} \cdot \nabla (\mathbf{B}_0 \cdot \mathbf{B}) + (\mathbf{v} \cdot \nabla \mathbf{B}) \cdot \mathbf{B}_0 + \mathbf{B} \cdot \nabla (\mathbf{B}_0 \cdot \mathbf{v}) - (\mathbf{B} \cdot \nabla \mathbf{v}) \cdot \mathbf{B}_0 \\
\dfrac{\partial \mathbf{B}_1}{\partial t} + \nabla \cdot (\mathbf{v}\mathbf{B} - \mathbf{B}\mathbf{v}) = -\nabla \cdot (\mathbf{B}_1 + \mathbf{B}_{01})\,\mathbf{v} - \dfrac{\partial \mathbf{B}_{01}}{\partial t}
\end{cases}
$$

$$
\mathbf{B} = \mathbf{B}_1 + \mathbf{B}_{00} + \mathbf{B}_{01}\,,\; E_1 = \frac{p}{\gamma - 1} + \frac{\rho \mathbf{v}^2}{2} + \frac{\mathbf{B}_1^2}{2}
$$

Haopeng Wang, Liping Yang, Poedts Stefaan et al. 2025a, SIP-IFVM: A time-evolving coronal model with an extended magnetic field decomposition strategy. ApJS, 278(59):1-17.

Time-evolving COCONUT

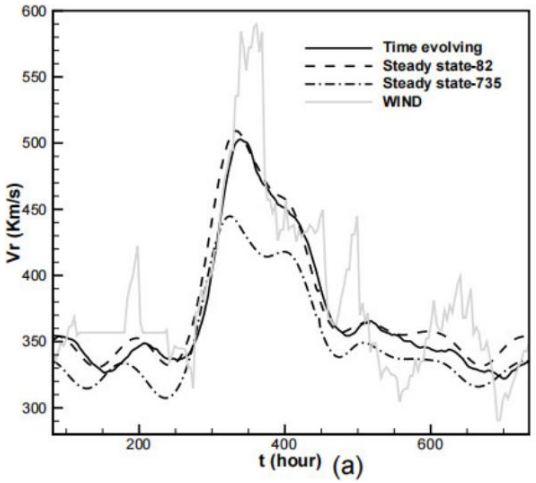

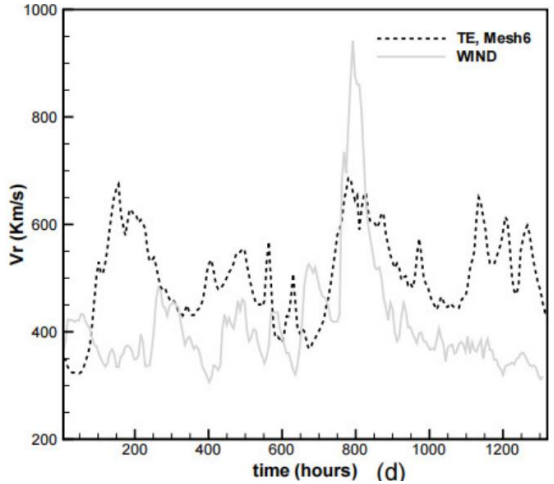

Timing diagram of the simulated and the observed radial velocity.

CR 2219 2220

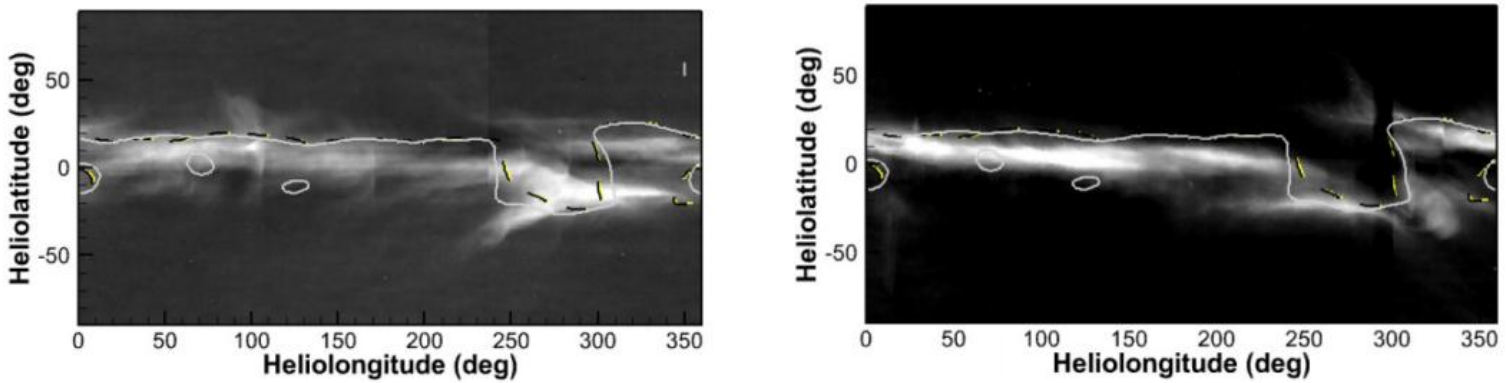

Solar minimum

Observed synoptic pB images and simulated magnetic neutral lines at $3R_s$.

Haopeng Wang, Stefaan Poedts, Andrea Lani et al.: 2025b, Efficient MHD modelling of the time-evolving corona by COCONUT. A &A, 694(A234):1-14.

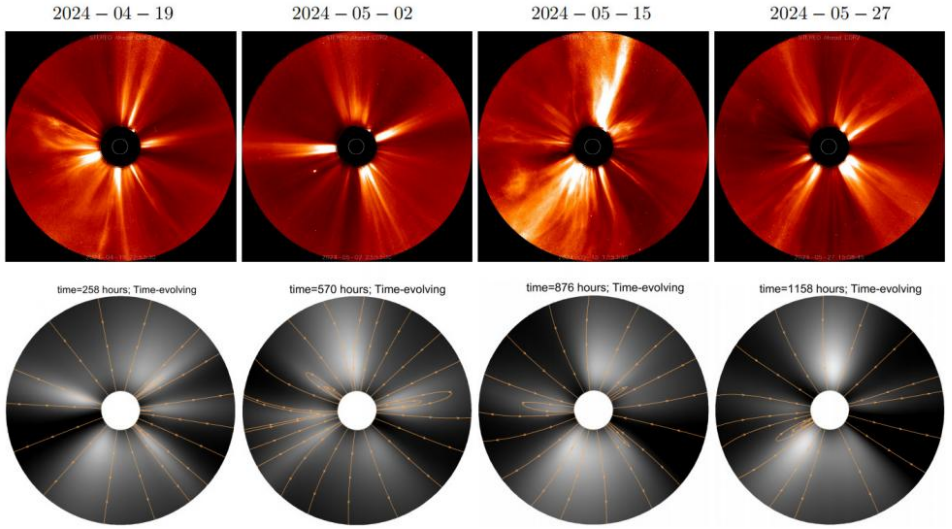

Solar maximum

Haopeng Wang, Stefaan Poedts, Andrea Lani et al.: 2025c, Time-evolving coronal modelling of the solar maximum around the solar storms in May 2024 by COCONUT. A&A:1-11.

STEREO-A COR2 pB observations and corresponding simulated pB images.

Time-evolving COCONUT

Table 1. Average relative differences between quasi-steady-state and time-evolving coronal simulation results.

Parameters	$RD^{t}_{ave,\rho}$	$RD^{t}_{ave,\lvert v\rvert}$	$RD^{t}_{ave,\lvert B\rvert}$
$t = 82\,h$	0.54%	1.06%	4.24%
$t = 735\,h$	4.53%	8.49%	35.35%

$$RD_{ave,\rho} = \frac{\sum_{i=1}^{N} \left|\rho_{i,QSS} - \rho_{i,TE}\right|}{\sum_{i=1}^{N} \rho_{i,QSS}},$$

$$RD_{ave,|\boldsymbol{v}|} = \frac{\sum_{i=1}^{N} \left|\boldsymbol{v}_{i,QSS} - \boldsymbol{v}_{i,TE}\right|}{\sum_{i=1}^{N} \left|\boldsymbol{v}_{i,QSS}\right|},$$

$$RD_{ave,|\boldsymbol{B}|} = \frac{\sum_{i=1}^{N} \left|\boldsymbol{B}_{i,QSS} - \boldsymbol{B}_{i,TE}\right|}{\sum_{i=1}^{N} \left|\boldsymbol{B}_{i,QSS}\right|}.$$

$$\begin{aligned} B_{BC,r}(t,\theta,\phi) = {} & h_{00}(t')\, B_r(\theta,\phi)_m \\ & + h_{10}(t')\,(t_{m+1} - t_m)\left(\frac{\partial B_r(\theta,\phi)}{\partial t}\right)_m \\ & + h_{01}(t')\, B_r(\theta,\phi)_{m+1} \\ & + h_{11}(t')\,(t_{m+1} - t_m)\left(\frac{\partial B_r(\theta,\phi)}{\partial t}\right)_{m+1} \end{aligned}$$

with $t' = \dfrac{t - t_m}{t_{m+1} - t_m}$.

Interpolated inner-boundary magnetic field for each time step

Table 2. Comparison of time-evolving coronal simulations with dt = 10 and 2 minutes for two CRs of physical time.

Wall-clock times for $dt = 2$ min & $dt = 10$ min (h)	$RD^{82\,hr}_{ave,\rho}$ & $RD^{735\,hr}_{ave,\rho}$	$RD^{82\,hr}_{ave,\lvert v\rvert}$ & $RD^{735\,hr}_{ave,\lvert v\rvert}$	$RD^{82\,hr}_{ave,\lvert B\rvert}$ & $RD^{735\,hr}_{ave,\lvert B\rvert}$
39.06 & 17.54	0.09% & 0.08%	0.10% & 0.09%	0.60% & 0.42%

Haopeng Wang, Stefaan Poedts, Andrea Lani et al.: 2025b, Efficient MHD modelling of the time-evolving corona by COCONUT. A &A, 694(A234):1-14.

Time-evolving COCONUT

Table 1. Average relative differences between variables calculated on the Nth- and fifth-level meshes.

Parameters	LV_N=6	LV_N=7
$RD^{LV_N}_{ave,\|B\|}$ at 3 R_s	21.96%	35.08%
$RD^{LV_N}_{ave,\|B\|}$ at 21.5 R_s	23.78%	43.32%
$RD^{LV_N}_{ave,\rho}$ at 3 R_s	0.50%	−1.17%
$RD^{LV_N}_{ave,\rho}$ at 21.5 R_s	−1.90%	−4.37%
$RD^{LV_N}_{ave,V_r}$ at 3 R_s	3.70%	6.94%
$RD^{LV_N}_{ave,V_r}$ at 21.5 R_s	3.22%	6.83%

$$RD^{LV_K}_{ave,\chi} = \frac{1}{N^{LV_K}} \sum_{i=1}^{N^{LV_K}} \frac{\chi^{LV_K} - \chi^{LV_5}}{\chi^{LV_5}}.$$

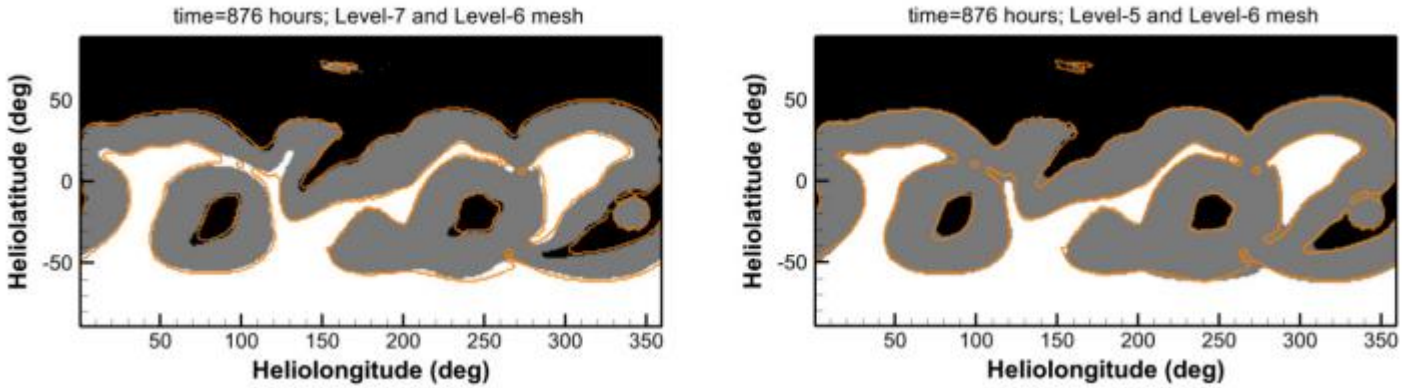

Contours of open- and closed-field regions at the 876th hour of the time-evolving simulations, performed on the seventh- (left) and fifth level (right) subdivided geodesic meshes, respectively. The orange lines overlaid on these contours denote the edge of close-field regions derived from the corresponding result on the sixth-level mesh.

Haopeng Wang, Stefaan Poedts, Andrea Lani et al.: 2025c, Time-evolving coronal modelling of the solar maximum around the solar storms in May 2024 by COCONUT. A&A:1-11.

Time-evolving COCONUT

Accurately determining solar wind parameters is crucial for Sun–Earth space research, as they significantly affect spacecraft safety and ground-based power systems. Traditionally, solar wind conditions are derived using coupled coronal and heliospheric models, with the latter initialized by the former's output at 0.1 AU, a computationally intensive and time-consuming process that limits real-time space weather forecasting. In this work, we propose a machine learning-based method for generating solar wind parameters at 0.1 AU. Specifically, we employ a U-Net neural network, trained using the output of the COolfluid COroNal UnsTructured (COCONUT) model as the learning target and Global Oscillation Network Group – Air Force Data Assimilative Photospheric Flux Transport (GONG–ADAPT) magnetograms as input. The model achieves correlation coefficients of 0.992 for radial velocity, 0.987 for number density, and 0.991 for radial magnetic field on the test set, with derived Alfvén speed and dynamic pressure reaching 0.996 and 0.769, respectively, demonstrating strong capability in reconstructing key solar wind parameters. Moreover, the model effectively captures the temporal evolution of these parameters within a single Carrington rotation. Once trained, the model generates full-surface solar wind predictions at 0.1 AU in 7.8 seconds on a CPU-only device and 0.065 seconds on a cluster with one GPU and 10 CPU cores, achieving 15× and 1800× speed-ups, respectively, over the COCONUT MHD simulation, which requires at least one hour to obtain a converged steady-state solution and over two minutes on 288 CPU cores per prediction.

Yucong Li, Haopeng Wang, Hyun-Jin Jeong et al.: Submitted to ApJS, Fast Reconstruction of Solar Wind MHD Parameters at 0.1 AU with Machine Learning.

Time-evolving COCONUT

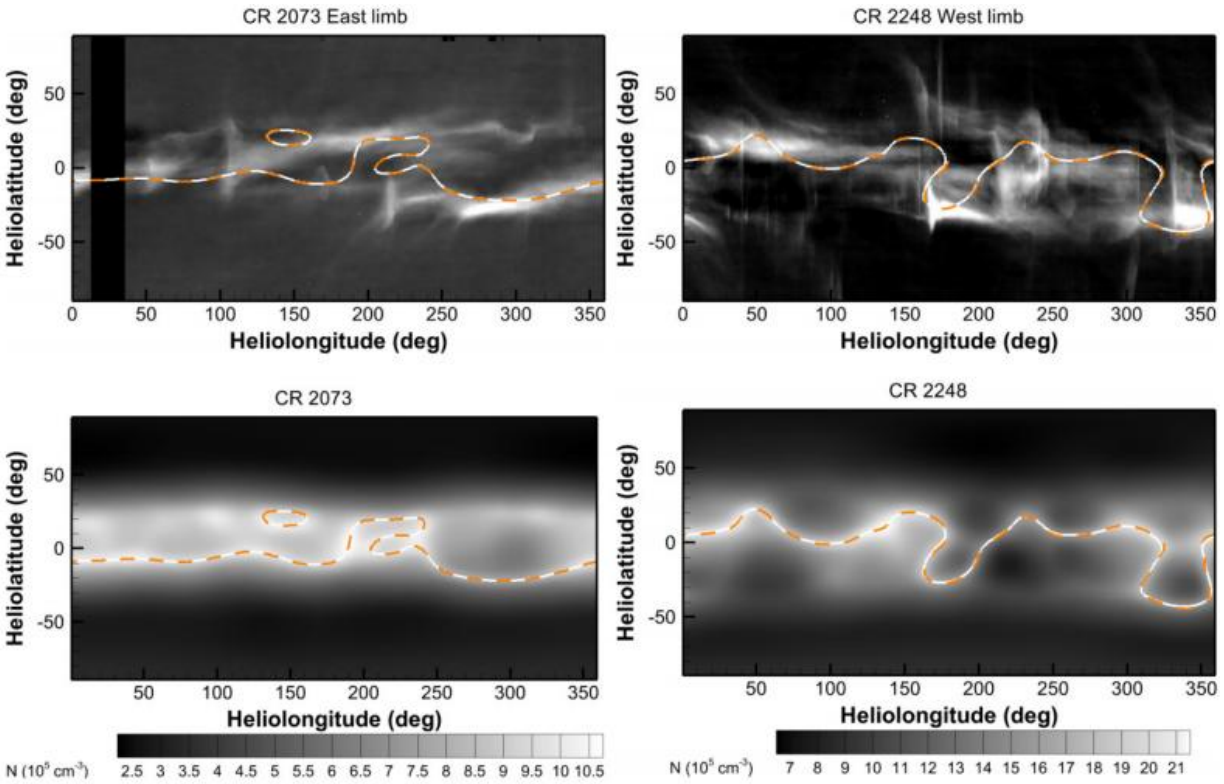

Observed Pb at 3 R_S and plasma density at 3 R_S simulated by COCONUT with decomposed energy equation.

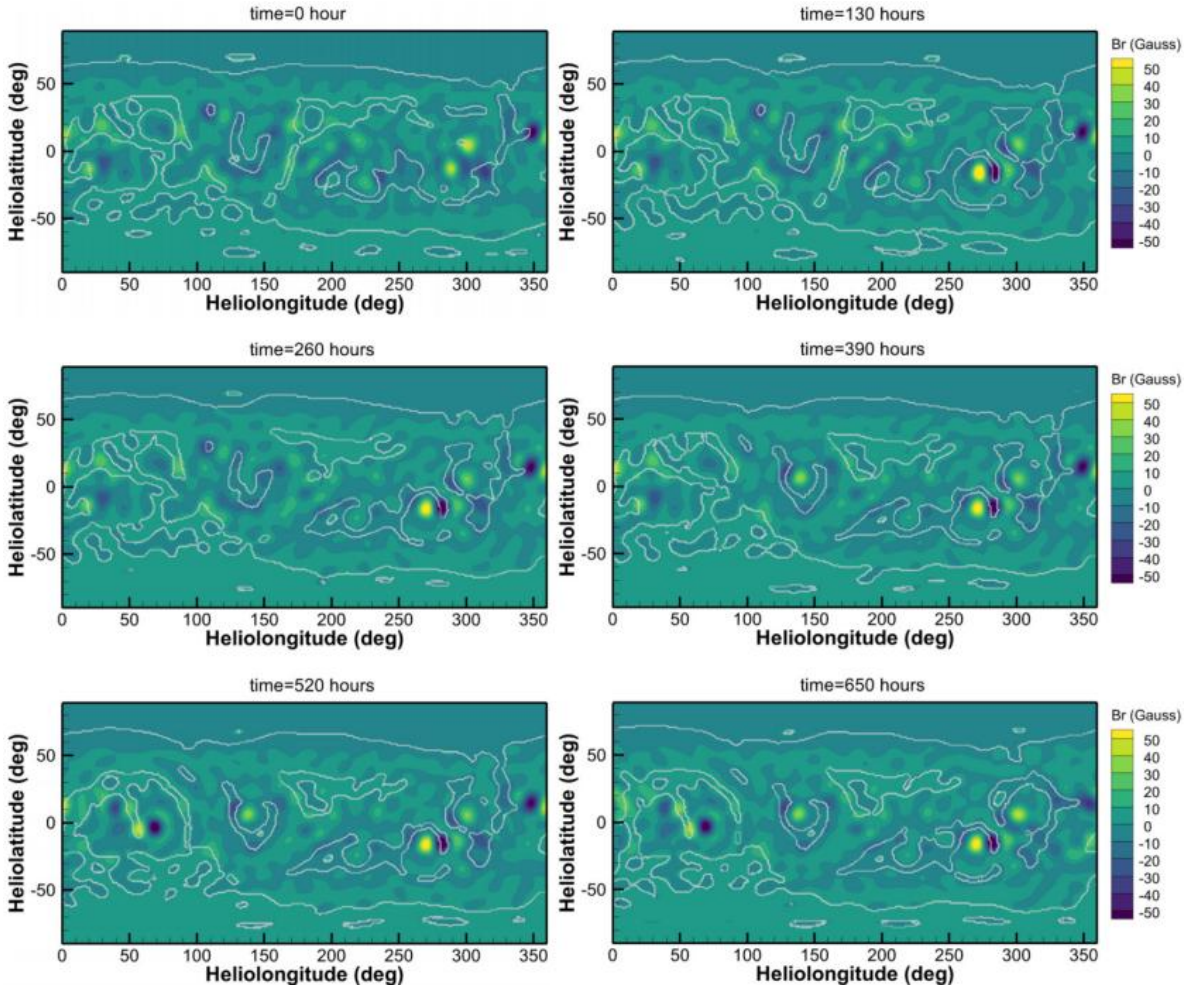

Time-evolving inner-boundary magnetic field and open-field regions for CR 2296 simulated by COCONUT with decomposed energy equation.

Wang et al. 2025.

Time-evolving COCONUT (1.5M cells, 360 CPUs, achieving ~24× speedup)

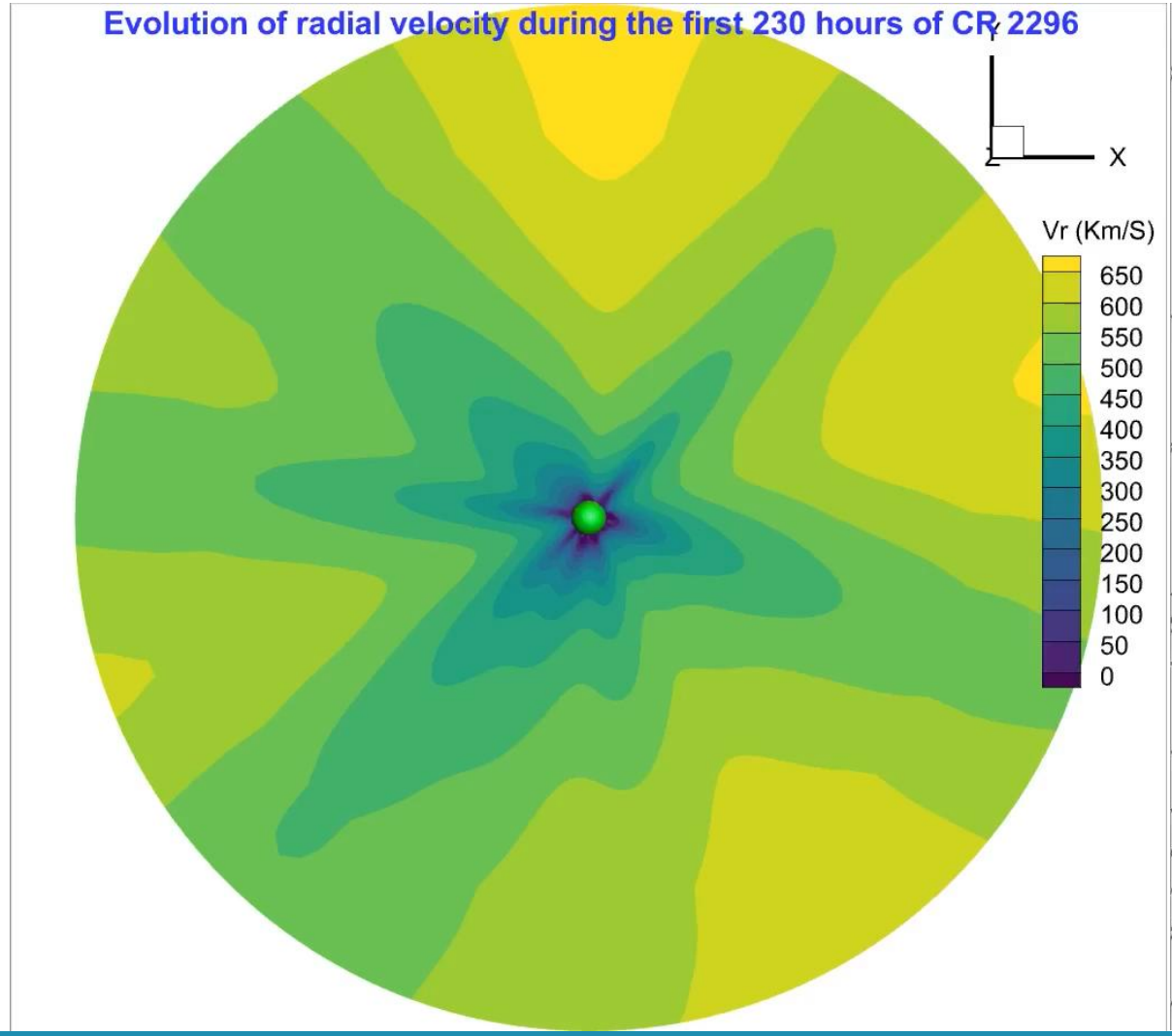

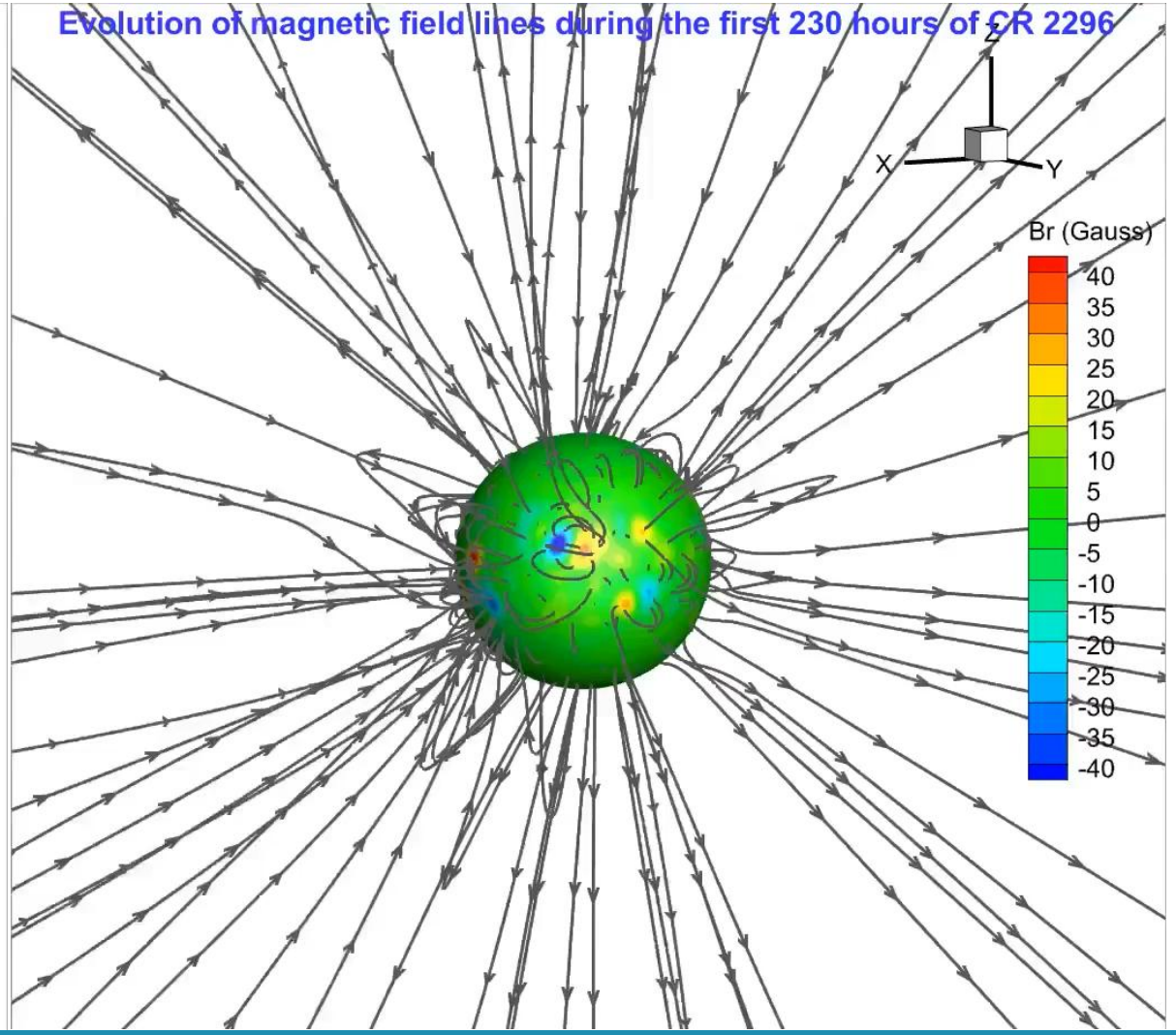

Time-evolving **SIP-IFVM** (~1M cells, 192 CPUs, achieving ~80× speedup)

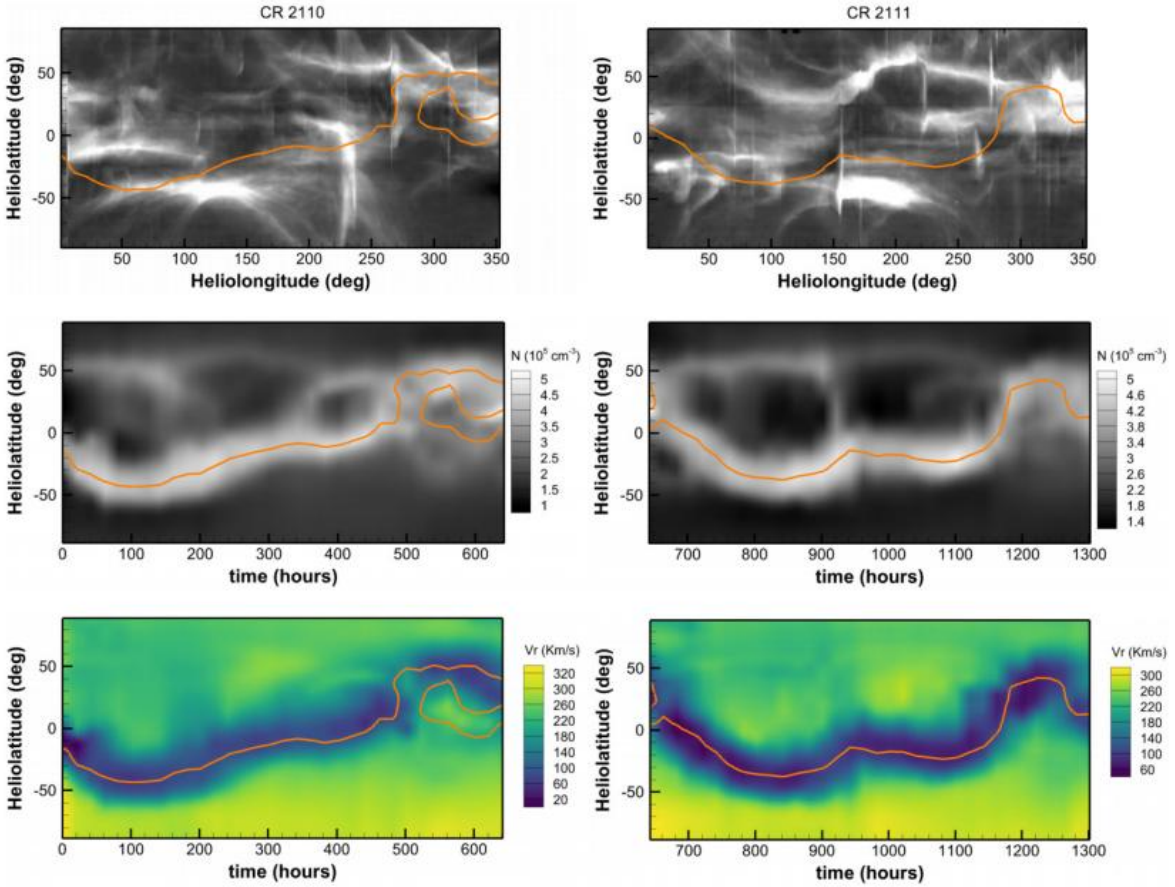

Synoptic maps of east-limb white-light pB images at 3 Rs observed by LASCO-C2/SDO, alongside the timing diagrams of simulated plasma number density and radial velocity at 3 R_s at the east-limb longitude of the Sun in the Earth view.

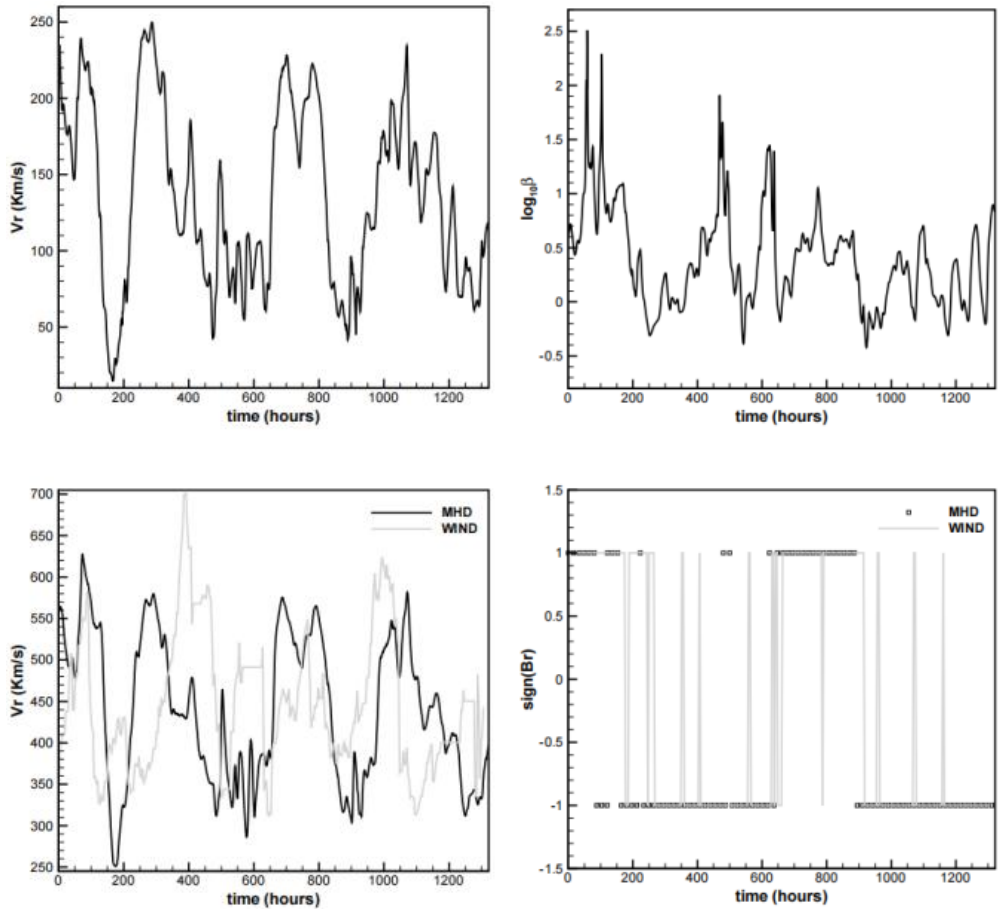

Timing diagram of radial velocity and decadic logarithms of plasma β or radial magnetic 5eld polarities at $3R_s$ (top) and 20 R_s (bottom).

Wang et al. 2025a.

Time-evolving **SIP-IFVM** (~1M cells, 192 CPUs, achieving ~80× speedup)

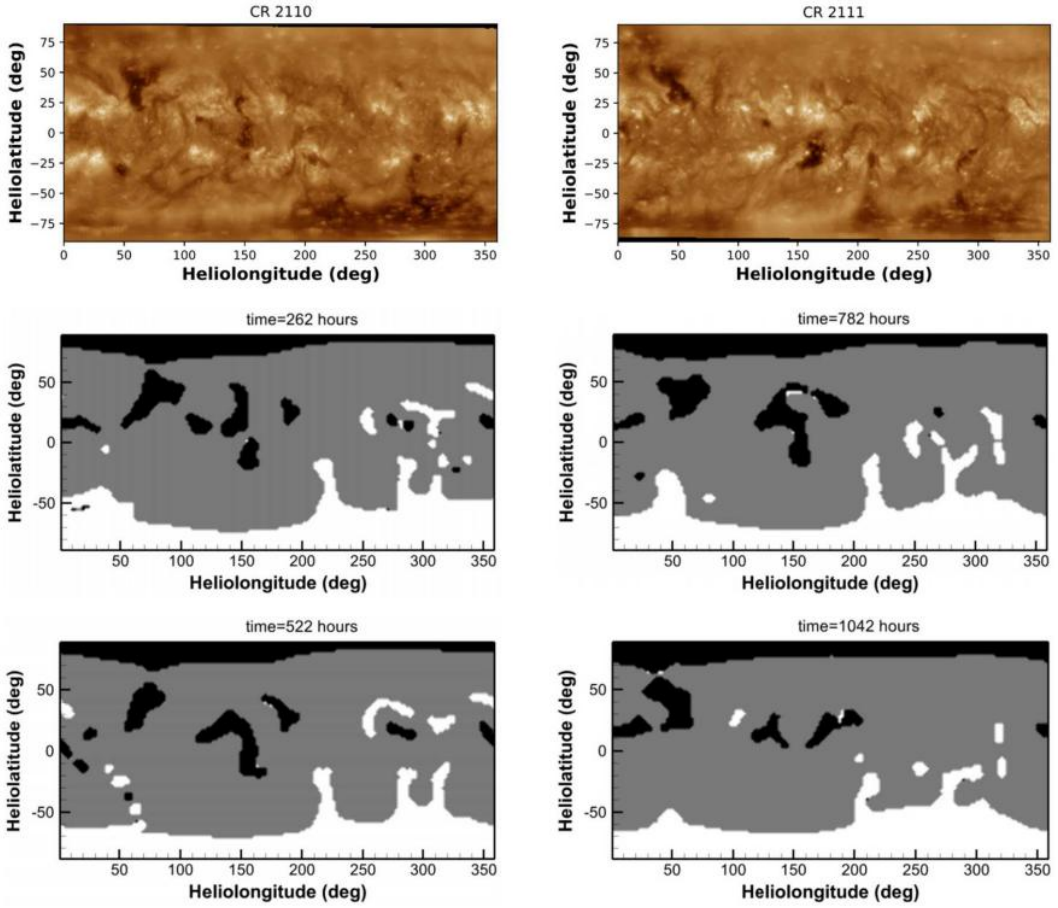

Synoptic maps of the EUV observations from the 193 Å channel of AIA/SDO, distributions of open- and closed-5eld regions modeled by the time-evolving SIP-IFVM coronal model

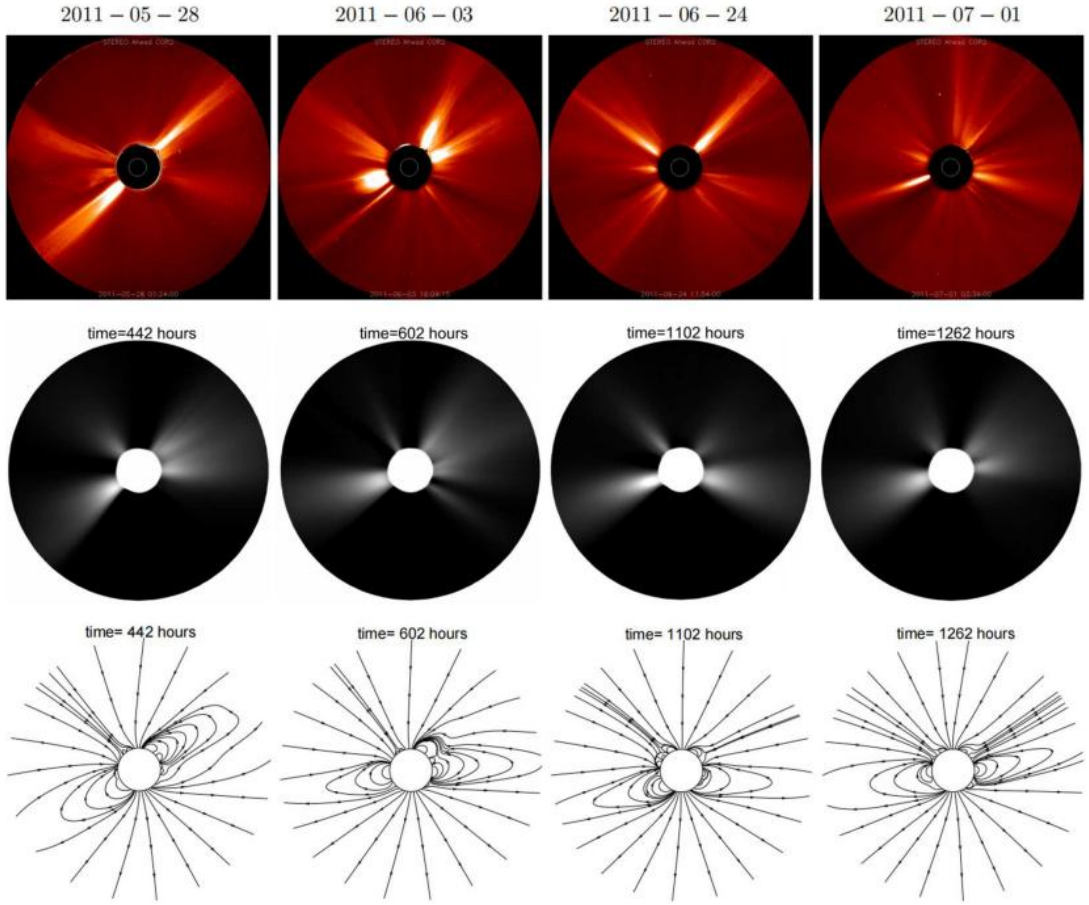

STEREO-A COR2 pB observations and corresponding simulated pB images and some selected simulated magnetic field lines.

Wang et al. 2025a.

Outline

- Fully implicit, time-evolving MHD coronal models **COCONUT** and **SIP-IFVM**
- **Faster-than-real-time MHD modeling of CME propagation through the sub-Alfvénic corona**

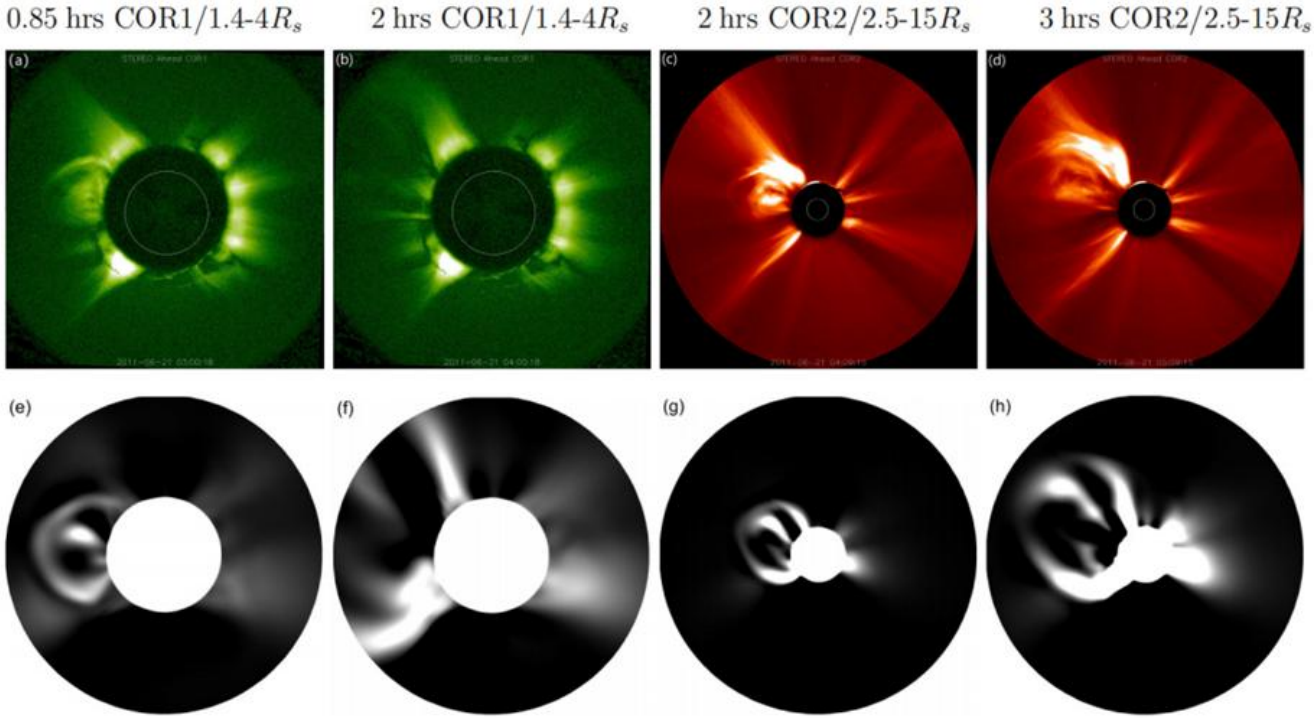

STEREO-A observation and CME simulation by **SIP-IFVM**

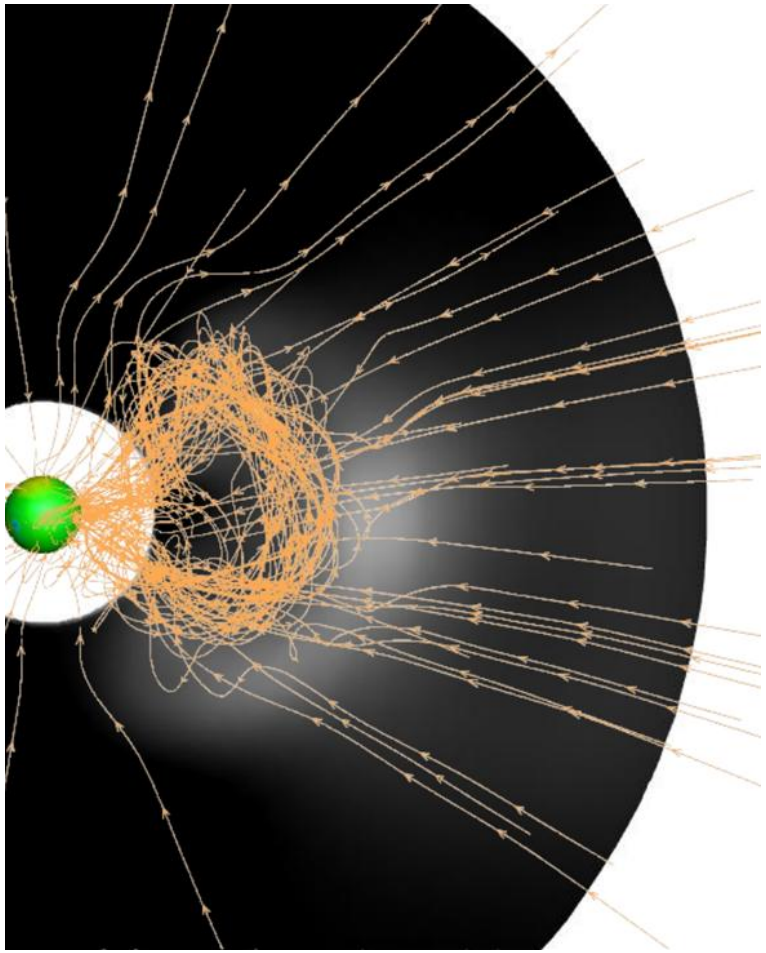

CME simulation by **COCONUT**

CME simulation in global background corona: **SIP-IFVM**

- Highly efficient: **Less than 1 hour** for background coronal and 6 hours of CME simulations (192 CPU cores, ~1M cells, from 1 R_s to 0.1 AU).
- Simulation results calculated at large time-step lengths can be consistent with those calculated at small time-step lengths.
- Results are basically **in agreement with the observations** from SDO, SOHO and STEREO-A/B.

Haopeng Wang, Jinghan Guo, Liping Yang et al.: 2025d, SIP-IFVM: Efficient time-accurate magnetohydrodynamic model of the corona and coronal mass eiections. A&A 693(A257):1-17.

Haopeng Wang, Jinghan Guo, Stefaan Poedts et al.: Accepted by ApJS, SIP-IFVM: An observation-based magnetohydrodynamic model of coronal mass ejection. 1-25, [arXiv:2506.19711].

CME simulation in global background corona: **SIP-IFVM**

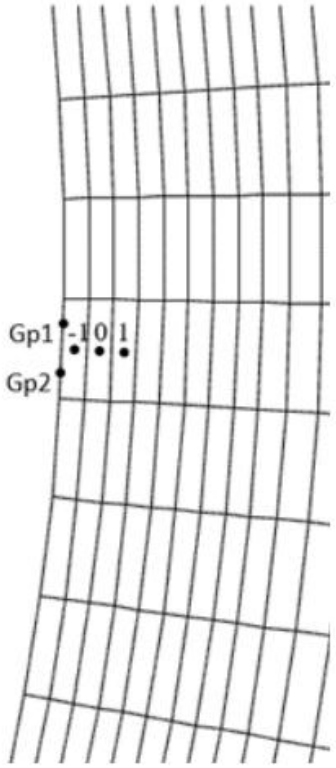

2D illustration of the inner boundary cells which lay on the left-most layer of this picture.

Initial magnetic field for CME propagation simulation ← $\mathbf{B}(\boldsymbol{x}) = \mathbf{B}_{FR}(\boldsymbol{x}) + \mathbf{B}_{BG}(\boldsymbol{x})$ → Background magnetic field

Regularised Biot-Savart Laws (RBSL) flux rope magnetic field

$$\mathbf{B}_{FR}(\mathbf{x}) = \nabla \times \mathbf{A}_I(\mathbf{x}) + \nabla \times \mathbf{A}_F(\mathbf{x})$$

$$\begin{cases} \mathbf{A}_I(\mathbf{x}) = \frac{\mu_0 I}{4\pi} \oint_{C \cup C^*} K_I(r)\mathbf{R}'(l)\frac{dl}{a(l)} \\ \mathbf{A}_F(\mathbf{x}) = \frac{F}{4\pi} \oint_{C \cup C^*} K_F(r)\mathbf{R}'(l) \times \mathbf{r}\frac{dl}{a(l)^2} \end{cases}$$

Wang et al. 2025d.

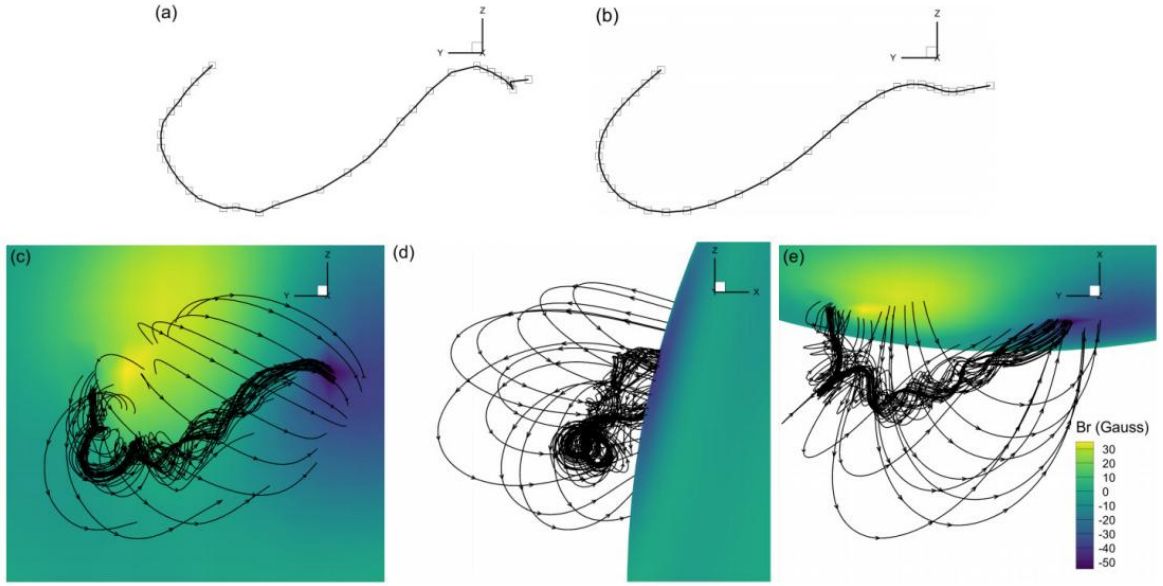

The RBSL flux rope axis path derived from the original observed (a) and the smoothed (b) sample points. (c, d, e) shows selected magnetic field lines of the flux rope and the background corona, viewed from three mutually perpendicular perspectives. (Wang et al. Accepted by ApJS)

CME simulation triggered by an analytical flux rope (Wang et al. 2025d)

Table 1. Comparation of CME simulations for 6 hrs of physical time t.

Parameters	$\chi = 1$	$\chi = 0.5$	$\chi = 0.25$	$\chi = 0.125$
wall-clock time (hours)	0.08	0.14	0.26	0.43
$RD^{\chi}_{ave,\rho}$ /RD^{χ}_{ave,V_r} at t=1hr	2.19%/1.54%	1.75%/1.16%	1.17%/0.72%	0.70%/0.40%
$RD^{\chi}_{ave,\rho}$ /RD^{χ}_{ave,V_r} at t=3hrs	3.23%/4.68%	2.24%/2.86%	1.59%/1.49%	1.14%/0.71%
$RD^{\chi}_{ave,\rho}$ /RD^{χ}_{ave,V_r} at t=5hrs	3.52%/4.29%	2.66%/2.33%	2.09%/1.18%	1.62%/0.64%

$$RD^{\chi}_{ave,\rho} = \sum_{i=1}^{N} \left| \rho_i^{\chi} - \rho_i^{CFL=1} \right| / \sum_{i=1}^{N} \rho_i^{CFL=1}$$

$$RD^{\chi}_{ave,V_r} = \sum_{i=1}^{N} \left| V_{ri}^{\chi} - V_{ri}^{CFL=1} \right| / \sum_{i=1}^{N} V_{ri}^{CFL=1}$$

$$\Delta t = \chi \cdot \tau_{flow}$$

τ_{flow} is a predefined reference time length, we set $\tau_{flow} = \kappa_1 \max\left(\min\left(\frac{R_S}{V_A}, \frac{R_S}{a_s}\right), \tau_{thre}\right)$, in which $V_A = \frac{B_{S-ave}}{\sqrt{\rho_S}}$ with B_{S-ave} denoting the average magnetic field intensity on the solar surface, and κ_1 and τ_{thre} denoting two adjustable reference parameters.

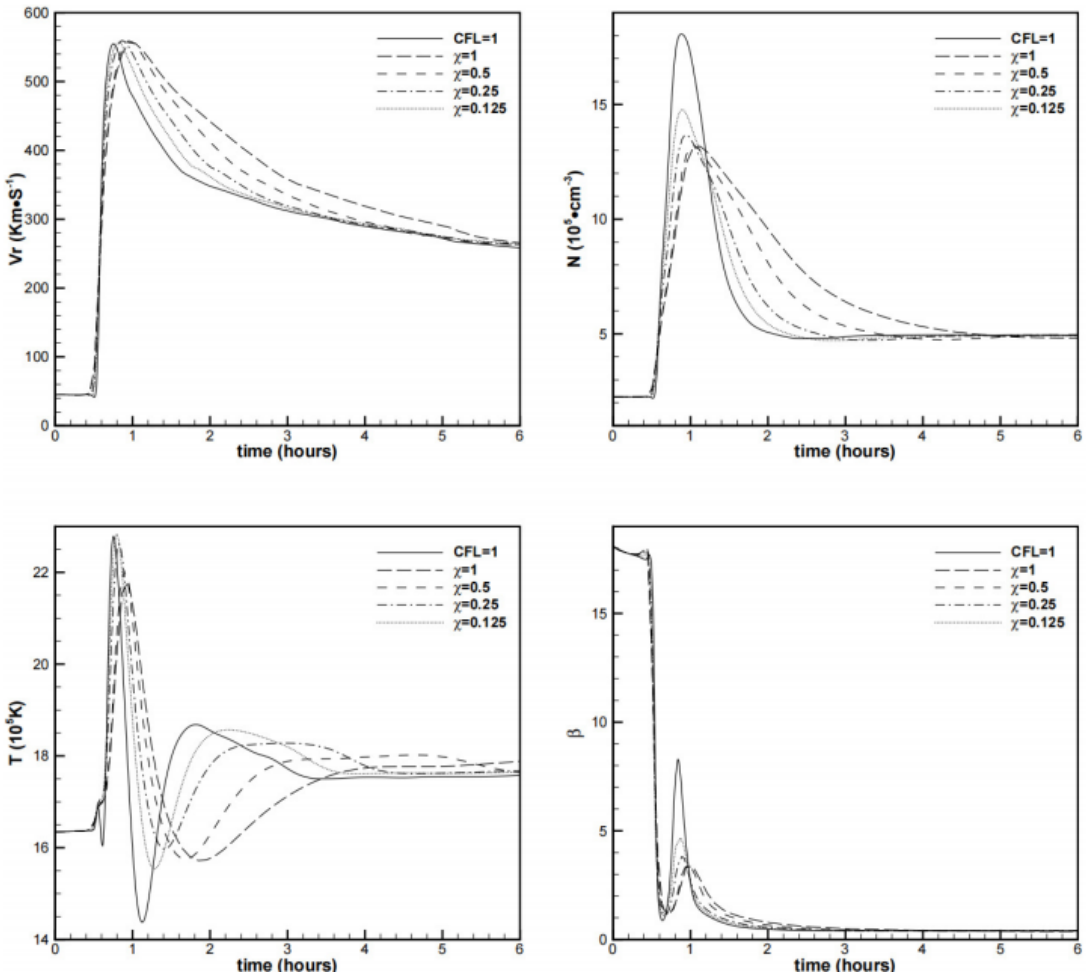

In situ measurements of simulated radial velocity Vr (km/s) (top left), proton number density (10^5/cm^3) (right top), temperature (10^5 K) and plasma β by the virtual satellite placed at (r, θ, φ) = (3Rs, 0°, 250°).

CME simulation triggered by observation-based flux rope (Wang et al. Accepted by ApJS)

ESDIRK2 and BDF2 pseudo-time marching method

Butcher table of a 2nd-order, three-stage ESDIRK2 method.

$a_{1,l}$	0	0	0
$a_{2,l}$	κ	κ	0
$a_{3,l}$	$1-b_2-\kappa$	b_2	κ
b_i	$1-b_2-\kappa$	b_2	κ

$$\mathbf{U}_i^{(1)} = \mathbf{U}_i^n$$

$$\frac{V_i}{\Delta t}\mathbf{U}_i^{(k)} = \frac{V_i}{\Delta t}\mathbf{U}_i^n - \sum_{l=1}^{k} a_{k,l}\mathbf{R}_i^{(l)}, \quad k = 2,3.$$

$$\mathbf{U}_i^{n+1} = \mathbf{U}_i^{(3)}$$

A pseudo time τ is introduced, the solution at these stages are obtained by solving a steady-state problem on τ.

$$V_i\frac{\partial \mathbf{U}_i^{(k)}}{\partial \tau} + \left(\frac{V_i}{\Delta t}\mathbf{U}_i^{(k)} - \frac{V_i}{\Delta t}\mathbf{U}_i^n + \sum_{l=1}^{k} a_{k,l}\mathbf{R}_i^{(l)}\right) = \mathbf{0}, \quad k = 2,3.$$

BDF2 integration method used to advance solution on τ until a steady state. An approximate temporal linearization helps to make the Jacobian matrix diagonally dominant.

$$V_i\frac{3\mathbf{U}_i^{(k,m+1)} - 4\mathbf{U}_i^{(k,m)} + \mathbf{U}_i^{(k,m-1)}}{2\,\Delta\tau^k} + V_i\frac{\mathbf{U}_i^{(k,m+1)} - \mathbf{U}_i^{(k,m)}}{\Delta t} + V_i\frac{\mathbf{U}_i^{(k,m)} - \mathbf{U}_i^n}{\Delta t} + a_{k,k}\left(\frac{\partial \mathbf{R}_i'}{\partial \mathbf{U}_i}\right)^{(k,m)}\left(\mathbf{U}_i^{(k,m+1)} - \mathbf{U}_i^{(k,m)}\right) =$$

$$-a_{k,k}\left(\frac{\partial \mathbf{R}_i'}{\partial \mathbf{U}_j}\right)^{(k,m)}\left(\mathbf{U}_j^{(k,m+1)} - \mathbf{U}_j^{(k,m)}\right) - a_{k,k}\mathbf{R}_i^{(k,m)} - \sum_{l=1}^{k-1} a_{k,l}\mathbf{R}_i^{(l)}, \quad k = 2,3$$

As $a_{k,k}$ approaches zero, the above equation becomes an explicit time integration scheme.

$$V_i\frac{3\mathbf{U}_i^{(k,m+1)} - 4\mathbf{U}_i^{(k,m)} + \mathbf{U}_i^{(k,m-1)}}{2\,\Delta\tau^k} + V_i\frac{\mathbf{U}_i^{(k,m+1)} - \mathbf{U}_i^{(k,m)}}{\Delta t} + V_i\frac{\mathbf{U}_i^{(k,m)} - \mathbf{U}_i^n}{\Delta t} + 1.1\left(\frac{\partial \mathbf{R}_i'}{\partial \mathbf{U}_i}\right)^{(k,m)}\left(\mathbf{U}_i^{(k,m+1)} - \mathbf{U}_i^{(k,m)}\right) =$$

$$-a_{k,k}\left(\frac{\partial \mathbf{R}_i'}{\partial \mathbf{U}_j}\right)^{(k,m)}\left(\mathbf{U}_j^{(k,m+1)} - \mathbf{U}_j^{(k,m)}\right) - a_{k,k}\mathbf{R}_i^{(k,m)} - \sum_{l=1}^{k-1} a_{k,l}\mathbf{R}_i^{(l)}, \quad k = 2,3$$

CME simulation triggered by observation-based flux rope (Wang et al. Accepted by ApJS)

Average relative differences between background coronal simulations calculated by the extended and conventional magnetic field decomposition approaches.

Parameters	$\mathrm{RD}_{\mathrm{ave},\rho}$	$\mathrm{RD}_{\mathrm{ave},V_r}$	$\mathrm{RD}_{\mathrm{ave},\lvert\mathbf{B}\rvert}$
magnitude	2.21%	1.06%	0.92%

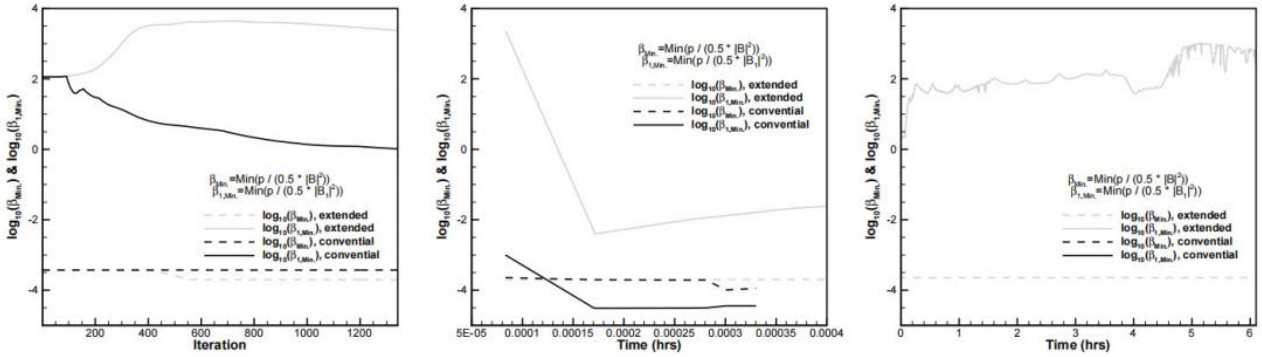

Evolution of the base-10 logarithms of the minimum values of $\beta_1 = \frac{p}{0.5,|\mathbf{B_1}|^2}$ and $\beta = \frac{p}{0.5,|\mathbf{B}|^2}$ within the entire computational domain, denoted by $\log_{10}(\beta_{1,\min})$ and $\log_{10}(\beta_{\min})$, respectively.

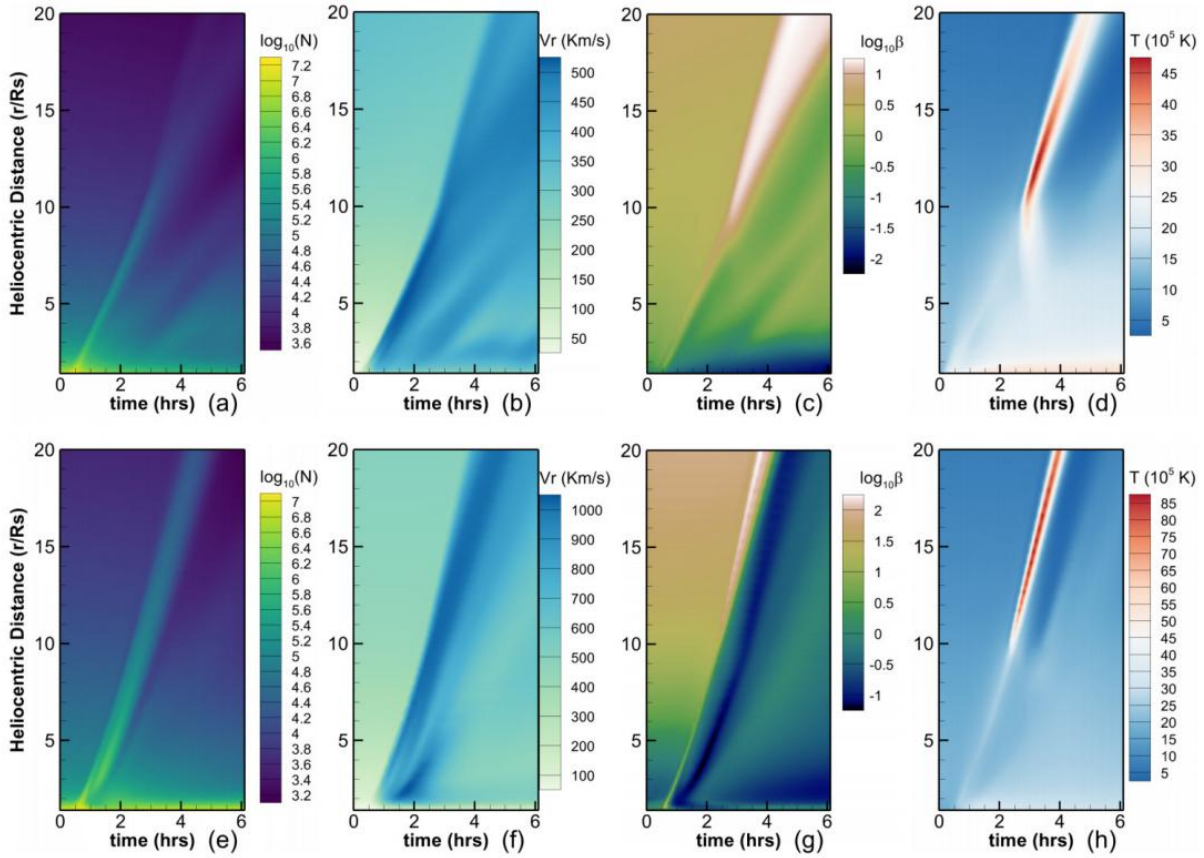

2 D timing diagrams of the base-10 logarithms of the simulated plasma number density, base-10 logarithms of plasma β and temperature T along two selected lines ranging from 1.4 Rs to 20 Rs over the first 6 hours the CME simulation.

CME simulation triggered by observation-based flux rope (Wang et al. Accepted by ApJS)

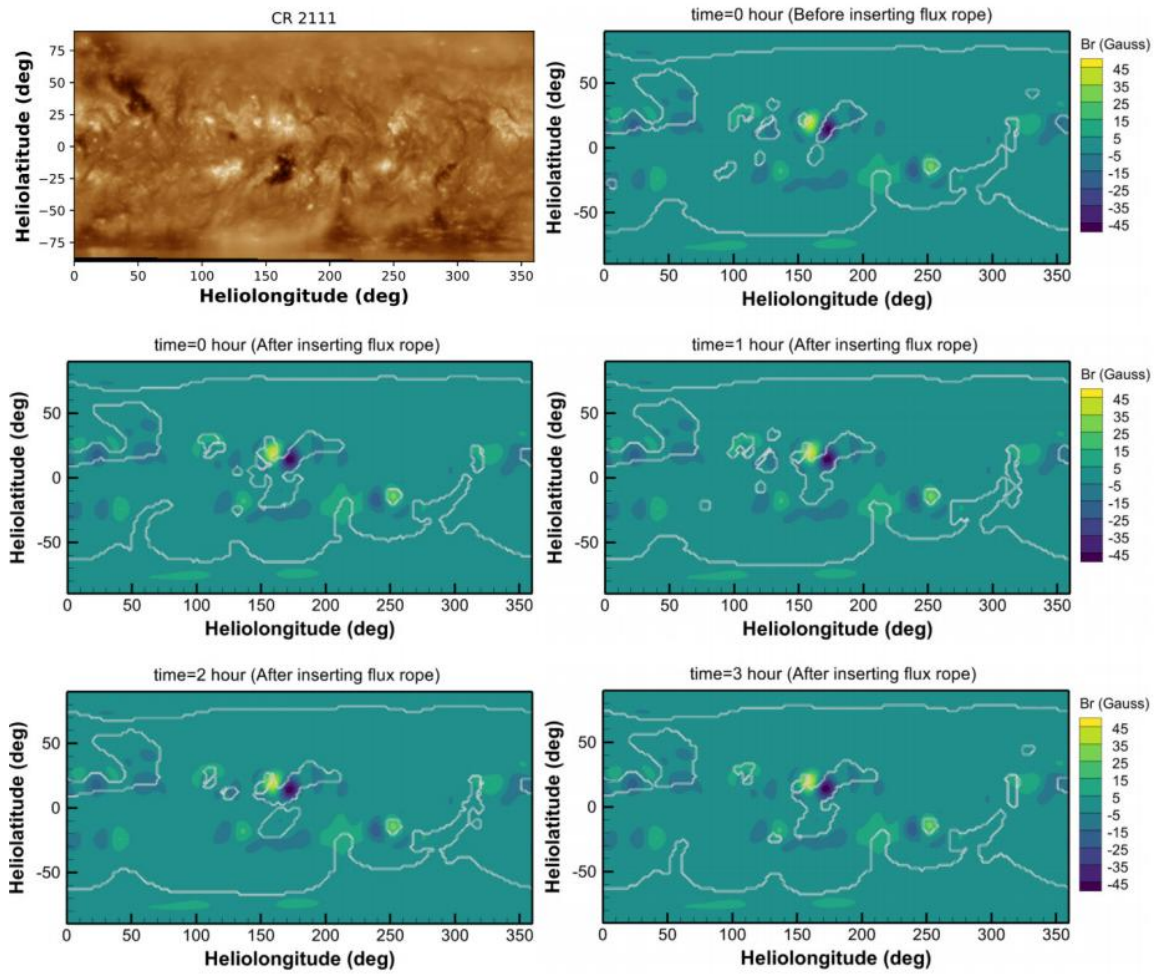

Radial magnetic field at 1.015 R_s overlaid with boundaries of the open-field regions, alongside the synoptic map of 193 Å EUV observations from AIA/SDO.

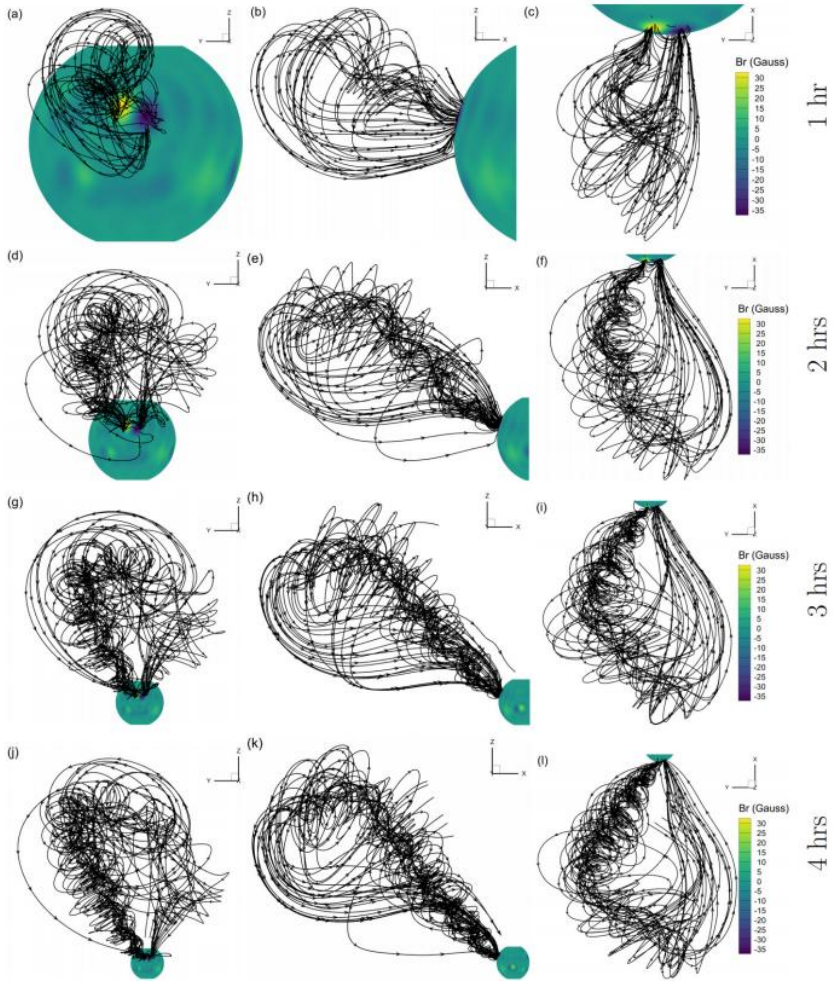

3D view of the magnetic field topology during the CME simulation.

CME simulation in global background corona: **COCONUT**

Employ the time-evolving COCONUT to simulate the CME events (in prep).

- The inner-boundary magnetic field also evolves during the CME propagation
- Evaluate the impact of coronal background evolution on CME propagation
- Conduct more realistic CME simulations

CME propagation calculated by time-evolving COCONUT

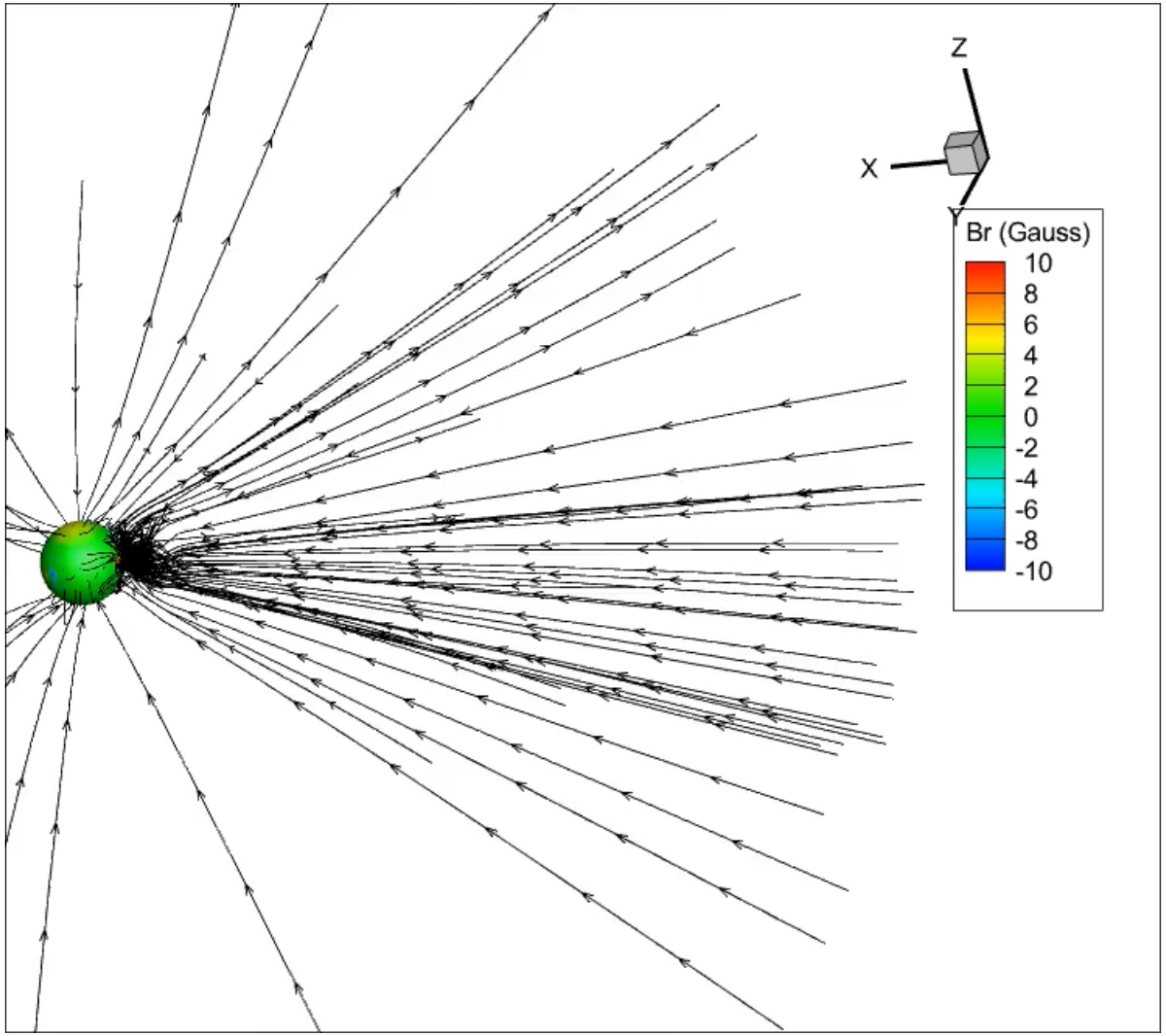

Evolution of simulated magnetic field lines in the time-evolving background corona.

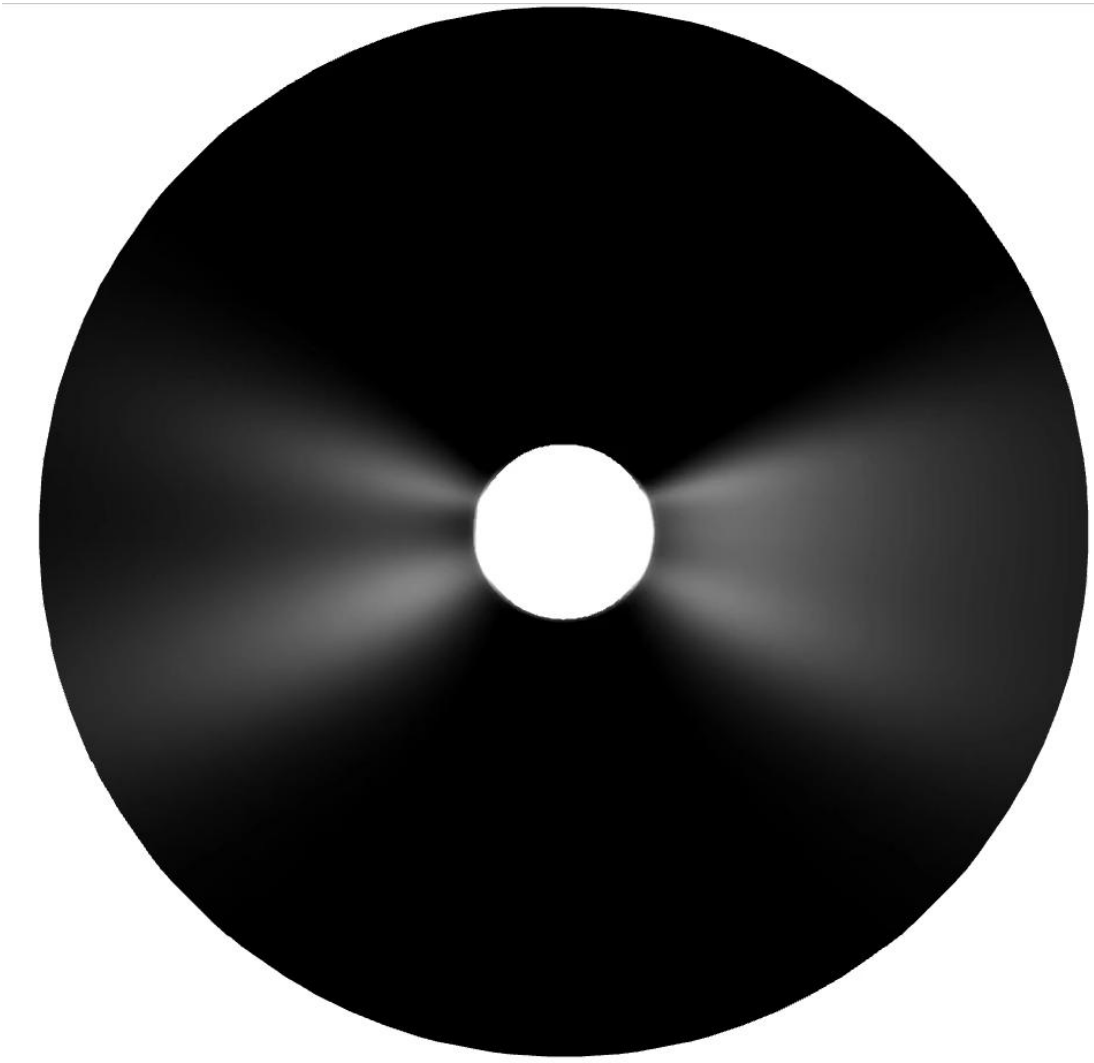

Evolution of simulated white-light pB image in the time-evolving background corona.

Conclusion and discussion

1. The implicit time-evolving coronal models COCONUT and SIP-IFVM show great promise for **practical space weather forecasting** due to their efficiency and stability. (Providing inner-boundary conditions for inner-heliosphere models, improve efficiency of CME simulations with required accuracy, …)

2. The extended magnetic field decomposition strategy and energy decomposition strategies improve the numerical stability of the MHD coronal and CME models in addressing **time-evolving low-β issues**.

3. We are **extending** the coronal model to 1 AU or **coupling** the coronal model with an inner heliosphere model to conduct some **faster-than-real-time** and more **realistic** CME simulations from the solar surface to 1 AU.

4. We plan to integrate active region models into global coronal model COCONUT.

Research works requiring collaborations

1. Add transient region, more self-consistent heating source terms
2. Incorporate AMR technique
3. Develop 3rd or higher order accurate algorithm
4. Utilize multiple observations to constrain and improve numerical simulation
5. Implement GPU acceleration
6. More convenient and intuitive visualization of the simulation results
7. Considering…?

Looking forward to more good ideas and comments

Thanks

E-mail: haopeng.wang1@kuleuven.be